

Insect-Spinach Waste Synergy: Enhancing *Cyamopsis tetragonoloba* under Copper Stress

Mehdi Afrouz,* Shadi Majd-Marani,* Hoda Zahedian, Fateme Arabnejad, Mohammad Taghi Alebrahim, Ali Eftekhari, Payman Azghani, and Te Ming Tseng*



Cite This: *ACS Omega* 2025, 10, 54302–54317



Read Online

ACCESS |



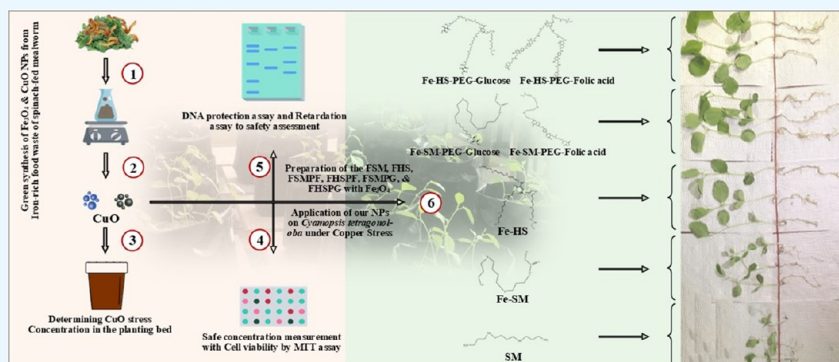
Metrics & More



Article Recommendations



Supporting Information



ABSTRACT: Fe₃O₄ nanoparticles (NPs) coated with hyperbranched spermine derivatives and functional groups such as glucose and folic acid, synthesized via green methods using rosemary extracts, represent a novel strategy to improve plant resistance to heavy metal stress. Various formulations, including FSM-coated (spermine), FHS-coated (hyperbranched spermine), FSMPF-coated (FSM-polyethylene glycol-folic acid), FSMPG-coated (FSM-P-glucose), FHSPF-coated (FHS-P-folic acid), and FHSPG-coated (FHS-P-glucose), were tested for their ability to improve the quality and stress resistance of Guar beans under copper oxide stress (CuO stress, CS). Six formulations (FSM, FHS, FSMPF, FSMPG, FHSPF, FHSPG) were synthesized and characterized by NMR, FTIR, TEM, SEM, DLS, and VSM. Compatibility and DNA protection were confirmed via electrophoresis. Greenhouse experiments showed that FSMPG and FHSPF significantly improved seedling growth, antioxidant enzyme activities, and nutrient uptake, particularly iron and nitrogen, under CuO stress. Cell suspension cultures of Guar were established to assess cytotoxicity of FHSPF2 and FHSPG1 NPs via trypan blue assay, revealing >80% cell viability up to 500 $\mu\text{g}/\text{mL}$. MTT assays on MCF-7 human breast cancer cells demonstrated excellent biocompatibility of FHSPF2 and FHSPG1 (>85% viability at 1000 $\mu\text{g}/\text{mL}$), while other variants showed moderate toxicity. Antibacterial tests against *Escherichia coli* and *Staphylococcus aureus* indicated mild activity only at the highest doses, with minimal impact at 500 $\mu\text{g}/\text{mL}$. Image analysis confirmed that callus morphology and growth were preserved, compared with the control. These results highlight the safe use of FHSPF2 and FHSPG1 NPs in agricultural biotechnology and biomedical applications, providing a sustainable approach to mitigate heavy metal stress and enhance plant resilience.

1. INTRODUCTION

Cyamopsis tetragonoloba (guar), a legume in the Fabaceae family, produces pods and is cultivated as an annual crop, although some varieties can persist as biennials or perennials. It can fix nitrogen in soil and restore nitrogen-depleted soils through crop rotation. Traditionally, it is used for food, fodder, laxatives, digestive aids, appetizers, and cooling agents. Thus, guar holds considerable economic importance. High-quality seeds and suitable soil conditions are essential for the optimum growth and development of Guar.^{1,2} Heavy metal pollution is one of the most critical environmental factors affecting plant growth, antioxidant enzyme activity, and hydrogen peroxide production. It causes oxidative cellular damage in plants by producing reactive oxygen species (ROS).³ Copper (Cu) is an essential micronutrient but becomes toxic at elevated

concentrations. The presence of essential heavy metals, such as Cu, in the soil causes plant phytotoxicity and stunted growth. At low levels, Cu is required for many biological and physiological functions in plants.⁴ In contrast, excess Cu increases the level of ROS in subcellular components, causing oxidative stress.

Received: July 14, 2025

Revised: September 30, 2025

Accepted: October 22, 2025

Published: November 3, 2025



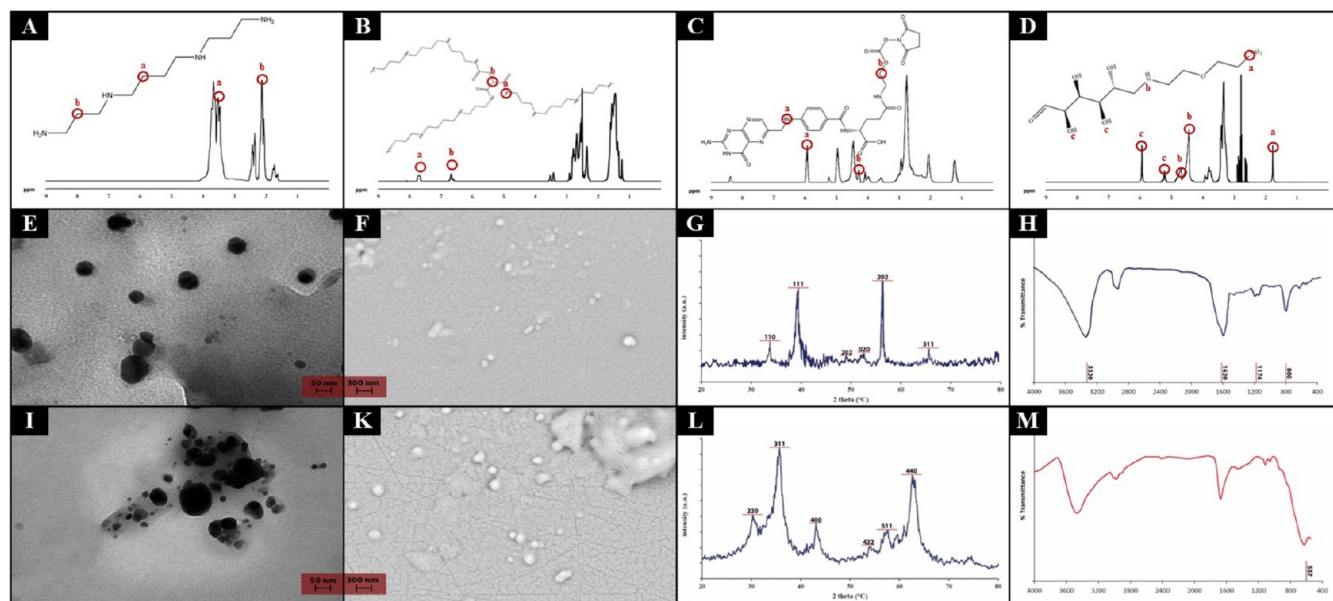


Figure 1. ^1H NMR spectroscopy of (A) SM, (B) HS, (C) PEG-FA, and (D) PEG-Glu. TEM characterization (E) CuO and (I) Fe_3O_4 . SEM characterization (F) CuO and (K) Fe_3O_4 . XRD, characterization (G) CuO and (L) Fe_3O_4 . FTIR characterization (H) CuO and (M) Fe_3O_4 . New figure prepared by the authors based on previously published data.²¹

As a result of Cu stress, Guar seedlings produce more antioxidant enzymes and proline. Due to their large surface area, nanoparticles (NPs) can reduce the detrimental impact of heavy metals on natural resources, thereby reducing their adverse effects on plant growth and yield. The green synthesis of iron oxide (Fe_3O_4) is a rapidly developing area within bionanotechnology, leveraging its enhanced surface area-to-volume ratio for improved plant physical, chemical, and biological functions.⁵ Although Fe_3O_4 nanoparticles are involved in metabolic processes, such as photosynthesis and DNA synthesis, their mechanisms of green synthesis remain poorly understood. Yellow mealworms (*Tenebrio molitor* L.), an agricultural pest, can convert spinach waste into high-value Fe_3O_4 nanoparticles, providing a sustainable approach to nanomaterial production.^{6,7} This approach aligns with circular economy principles by converting mealworm waste into products with applications in food science, technology, and sustainable chemistry. Furthermore, Fe_3O_4 NPs have demonstrated efficacy in mitigating oxidative stress in plants, reducing H_2O_2 and MDA levels, and enhancing SOD and POD activities. Exploring mealworm-derived Fe_3O_4 nanoparticles thus provides a dual advantage: sustainable waste management and improved plant stress resilience.^{8,9} The NPs increased corn germination rates, mean germination time, and plant growth.¹⁰ Micronutrients are essential for germination and growth, and polyamines (PAs) enhance plant tolerance to abiotic stresses. As a class of growth substances, PAs are small organic polycations common in living organisms and include spermidine, spermine, and putrescine, which are all critical for plant development and growth.^{11,12}

The levels of PAs and abiotic factors affect PAs biosynthesis and metabolic pathways; therefore, PAs could be excellent targets for improving plant tolerance to abiotic stress. Using spermine under heavy metal stress improved wheat performance, according to research.¹³ Spermine is also necessary to control physiological processes, such as cell division, embryogenesis, floral emergence, leaf senescence, and abiotic stress.^{13,14} Heavy metal stress can be minimized by using

spermine and iron together, according to research.¹² Additionally, Guar's growth conditions in nature are variable, making chemical stability crucial. Researchers used PEG-polyspermine bound with PEG, glucosamine, and folic acid to stabilize the NPs' size, as polyspermine showed great potential in protecting certain enzymes.^{15,16} The positive charge of these polycations also makes them electrostatically attractive to polyanions. Biocompatible, hydrophilic, and neutral NPs coat elicitor surfaces to increase their solubility. Therefore, ligand-functionalized NPs deliver polyspermine more efficiently to the target Guar cells. The conjugation of spermine with Guar-cell-specific transporters, such as glucose and folic acid, will enhance their penetration into the cell and improve the xylem or phloem residence time, given that glucose and folic acid are crucial and beneficial factors in plant growth and development.^{17–19}

A wide range of multifunctional NPs has now become possible with the rapid advancement of nanotechnology. Thus, the objective of this research was to develop and synthesize multifunctional NPs. For this purpose, Fe_3O_4 NPs and copper oxide (CuO) were extracted from the hydroalcoholic extract of food waste powder of the insect larvae mealworms (*Tenebrio molitor* L.), which were exclusively fed on spinach leaves (*Spinacia oleracea*). Then, Fe_3O_4 NPs surfaces were coated with spermine and hyperbranched spermine linked by Glucose-polyethylene glycol amine (NH_2 -PEG-Glu) and Folic acid-polyethylene glycol amine (NH_2 -PEG-FA) to increase copper oxide (CuO) stress tolerance in plants.

2. MATERIALS AND METHODS

Detailed experimental procedures are provided in the Supporting Information. See the Supporting Information Information for experimental details and additional data.

3. RESULTS AND DISCUSSION

3.1. Preparation and Characterization of the NPs.

3.1.1. NMR Analysis of Our NPs (SM, HS, PEG-Folic Acid,

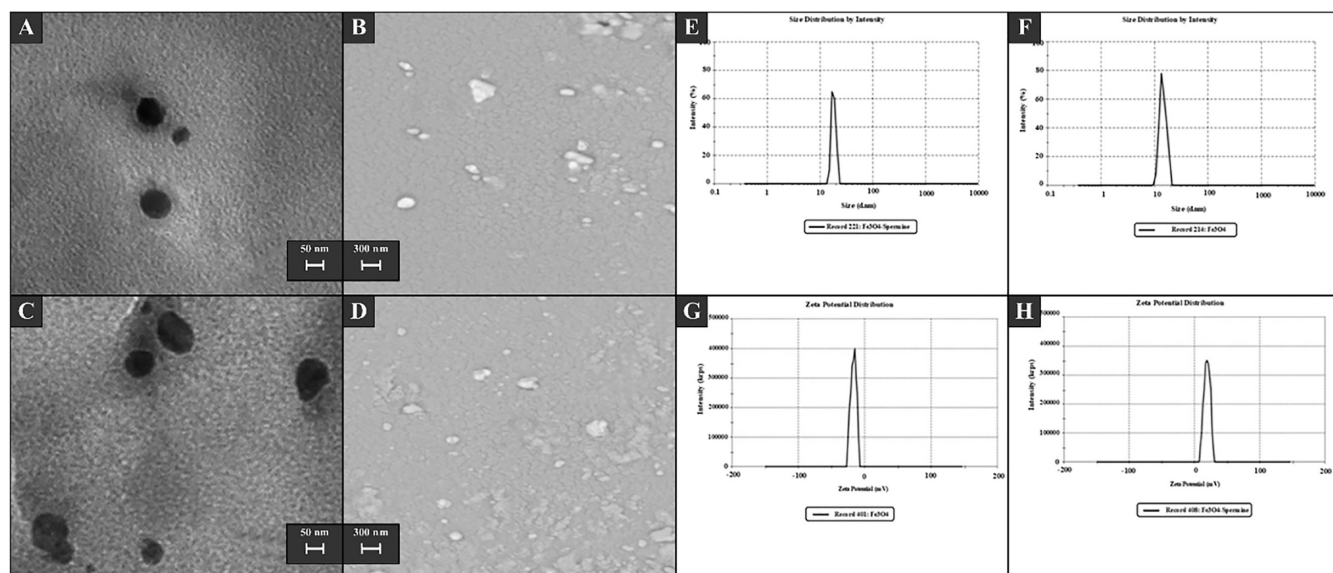


Figure 2. TEM images of the Fe₃O₄ (A), SEM images of the Fe₃O₄ (B), TEM images of the Fe₃O₄-SM NPs (C), SEM images of the Fe₃O₄-SM NPs (D). DLS results of Fe₃O₄ and Fe₃O₄-SM NPs: (E, F) zeta potential of the Fe₃O₄-SM and Fe₃O₄ NPs respectively, and (G, H) particle size of Fe₃O₄ and Fe₃O₄-SM NPs respectively; New figure prepared by the authors based on previously published data.^{21,23,24}

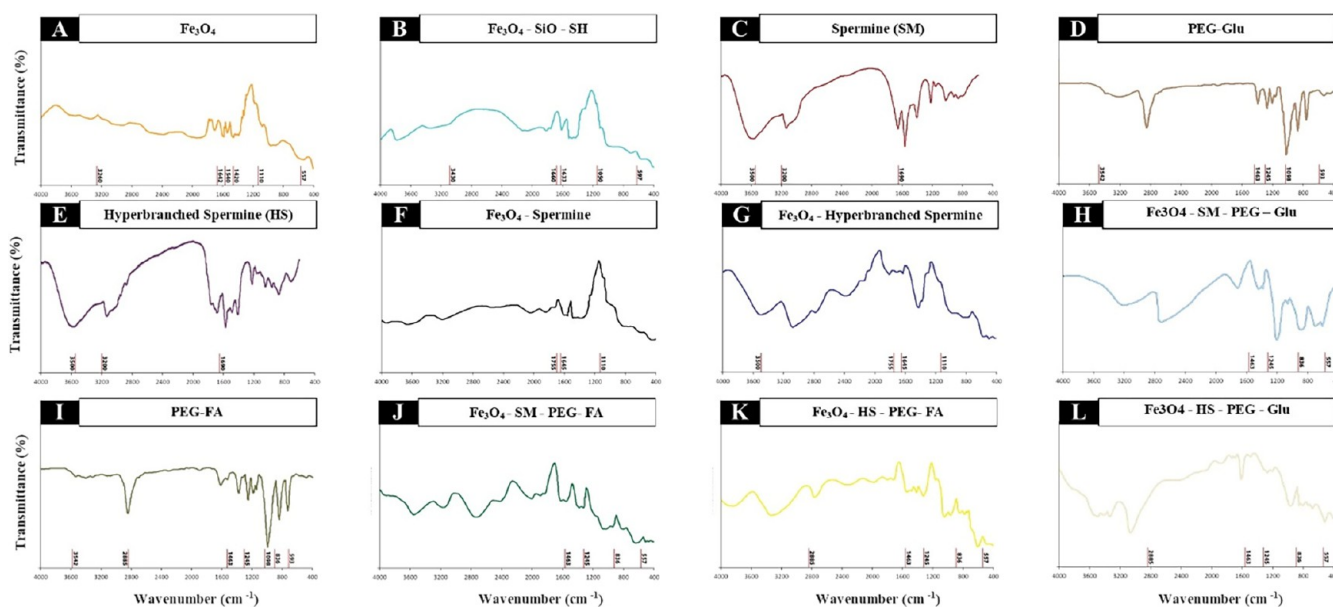


Figure 3. FTIR spectra of FSM, FHS, FSMPF, FHSPE, FSMPG, and FHSPG NPs; New figure prepared by the authors based on previously published data.^{21,28}

PEG-Glucose), along with Characterization of Fe₃O₄ and CuO NPs Extracted from MSFW. We elucidated the structural components of SM, HS, NHS-PEG-FA, and Glu-PEG-NH₂ by using ¹H NMR analysis, along with the structural components of the Fe₃O₄ and CuO NPs extracted from MSFW by using transmission electron microscopy (TEM), scanning electron microscopy (SEM), X-ray diffraction (XRD), and Fourier transform infrared spectroscopy (FTIR). ¹H NMR spectra of NPs showed peaks at 1.7 and 2.6 ppm related to hydrogen (a and b) in SM, the peaks at 7.7 and 6.7 ppm related to hydrogen (a and b) in HS, the peaks at 6.1 and 4.2 ppm related to hydrogen (a and b) in NHS-PEG-FA, and the peaks at 1.8, 4.5, and 5.9 ppm related to hydrogen (a, b, and c) in Glu-PEG-NH₂; that related to hydrogen bonds from connections in the structure of these materials are like pentane-1,3,5-tricarboxylic

acid, methylene (-CH₂-), and aromatic protons (Figure 1A-D). TEM and SEM were used to investigate the crystalline structures of the Fe₃O₄ and CuO NPs. These results show that the Fe₃O₄ NPs have a spherical shape with a smooth surface and a nonuniform distribution (Figure 1I,K). This dual redox role of the MSFW extract enabled the formation of stable CuO and Fe₃O₄ NPs with controlled oxidation states. In contrast, CuO NPs have a spherical shape and uniform distribution (Figure 1E,F). The nanoparticles measured 10–20 nm in size, as determined using ImageJ software. The morphology of NPs has a substantial impact on their properties and dispersibility in plants. According to past research, spherical NPs have a higher transfer rate to cells than do other NPs morphologies. Comparison of Miller indices in some XRD peak values on Fe₃O₄ (i.e., 220, 311, 400, 511, and 440, that respectively

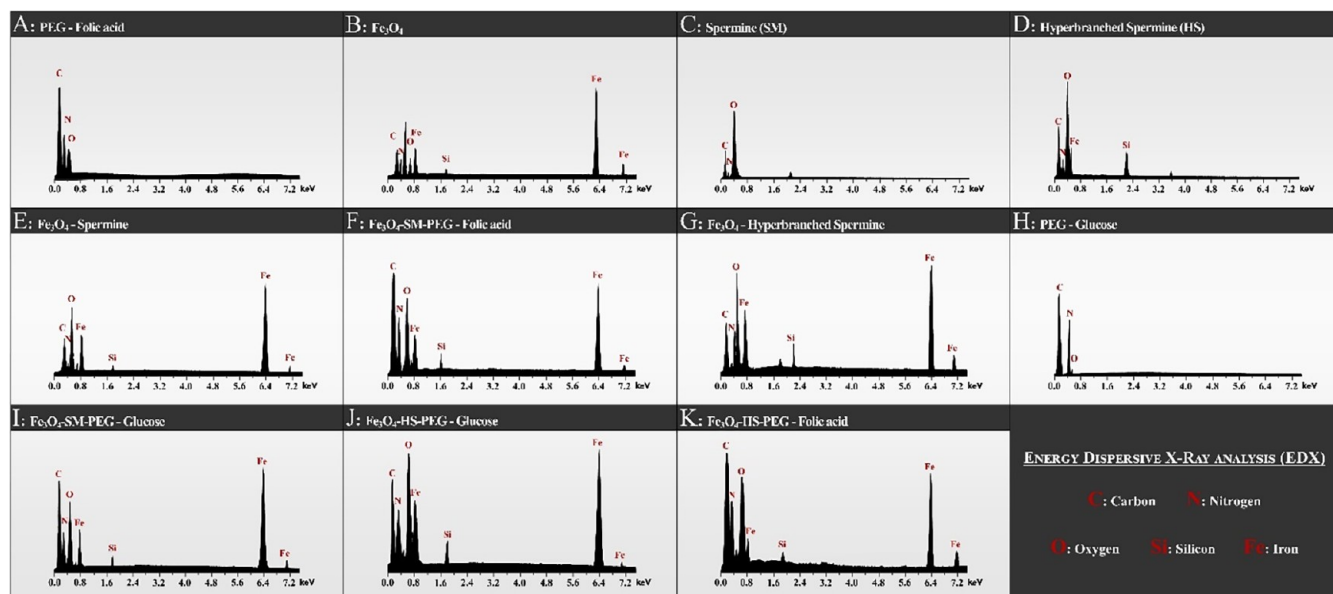


Figure 4. (A–K) EDX curves of NPs; New figure prepared by the authors based on previously published data.²⁸

correspond to the angles 30.9, 35.9, 43.8, 57.7, and 62.9°) and CuO NPs (i.e., 110, 111, 202, 020, 202, and 311 that respectively correspond to the angles 34.5, 39, 49.2, 53.4, 58.9, and 66.9°), in addition to confirming the correct synthesis of Fe₃O₄ (Figure 1L) and CuO NPs (Figure 1G), indicates the small size of the synthetic NPs according to broadening of the XRD peaks. Also; According to the peaks at 575 cm⁻¹ (the tensile vibration of the octahedral Fe–O structure) and 2931 cm⁻¹ (the C–H bond tensile vibration from Fe₃O₄ NPs), with along the peaks at 1556, 2952, and 3420 cm⁻¹ (the tensile vibration of the octahedral Cu–O structure) in the FTIR analysis diagram, we confirmed the synthesis of the Cu–O (Figure 1H) and Fe₃O₄ (Figure 1M) NPs.^{2,8,12,20}

Previous studies have demonstrated that Fe₃O₄ and Fe₃O₄–SM NPs exhibit a predominantly spherical morphology with sizes ranging from 10 to 40 nm, as confirmed by both TEM and SEM imaging (Figure 2). Coating with spermidine resulted in a slight increase in particle size and the formation of oval-shaped structures, which aligned with earlier observations. DLS analysis supported these results, showing an average hydrodynamic diameter of 17 ± 3 nm for Fe₃O₄, which increased to 23 ± 16 nm after coating with spermine. Additionally, the surface charge changed from -3.2 ± 0.35 to +18.42 ± 3.2 mV, attributed to the presence of cationic amine groups in spermine. The small particle size and enhanced positive surface charge have been reported to facilitate a more efficient cellular uptake, particularly in plant cells. These findings provide a reference framework for the ongoing investigations in the present study.^{2,11,12,22}

3.1.2. Characterization of Our NPs. Figure 3 shows the FTIR analysis of Fe₃O₄@SiO₂–SH, FSM, FHS, FSMPF, FHSPF, FSMPG, and FHSPG NPs. Accordingly, the peak at 11050 cm⁻¹ related to the Si–O bond of Fe₃O₄@SiO₂–SH, the peak at 3200 and 3500 cm⁻¹ related to the N–H vibrations bond (primary and secondary amines) of SM and Hs, the peak at 3200–3500 and 1690 cm⁻¹ related to the C–N and C=O groups of Hs, the peak at 1645–1755 cm⁻¹ associated with the amino groups of Fe₃O₄@SiO₂–SS–SM and Fe₃O₄@SiO₂–SS–HS (that indicate for confirming SM and HS conjugate with Fe₃O₄@SiO₂–SS–COOH), and the peak at 1645 to 1755 cm⁻¹

related to the amide and amide amino groups or the peak at 948 and 1348 cm⁻¹ related to the C–H and C–O–C bonds of FSM, FHS, FSMPF, FHSPF, FSMPG, and FHSPG (that indicate for confirming PEG-folic acid and PEG-glucose conjugate with Fe₃O₄@SiO₂–SS–SM and Fe₃O₄@SiO₂–SS–HS), indicating that materials were successfully grafted to the polymer (NPs) (Figure 3).^{2,12,20,25–27}

We elucidated the structural components of our NPs using magnetic behavior analysis (MBA), thermogravimetric analysis (TGA), ultraviolet–visible spectroscopy (UV–vis), and energy-dispersive X-ray analysis (EDX). For Fe₃O₄ NPs, the saturation magnetization was 41.3 emu/g (Figure 7I). However, after being coated with SM, HS, PEG-folic acid, and PEG-glucose, Fe₃O₄ NPs saturation magnetization decreased significantly from 46.8 to 40.2 emu/g (related to FSM), 38.1 (related to FHS), 25.8 emu/g (related to FSMPF), 20.9 emu/g (related to FHSPF), 23.7 (related to FSMPG), and 21.9 emu/g (related to FHSPG). Encapsulation of magnetic nanoparticles in biodegradable coatings typically reduces their saturation magnetization. These data agreed with those in the previous report. Considering the two stages of degradation in the TGA curves for Fe₃O₄ NPs and several steps of degradation for FSM, FHS, FSMPF, FHSPF, FSMPG, and FHSPG NPs, it may be concluded that structures such as FSM, FHS, FSMPF, FHSPF, FSMPG, and FHSPG NPs contain more compounds than Fe₃O₄ NPs (Figure 7K). By carefully examining the results of this diagram, it can be understood that the temperature resistance of Fe₃O₄ NPs decreased significantly after they were modified with SM, HS, PEG-FA, and PEG-Glucose. Our results were consistent with the data received from the UV/vis curve. Increased absorption, reflected in UV–vis spectra, reduces light transmission through the solution. So, NPs are synthesized and stable, as demonstrated in image C. The SM, HS, PEG-FA, and PEG-Glucose did not show any visible peak, but the UV/vis spectra showed that Fe₃O₄–Si peaks at 360–400 nm were sharply reduced, and the FSM, FHS, FSMPF, FHSPF, FSMPG, and FHSPG NPs peaks at 330–500 nm sharply decreased because of the binding of spermine on the Fe₃O₄@SiO NPs surface (Figure 7J). The energies N–O were shown to be present in

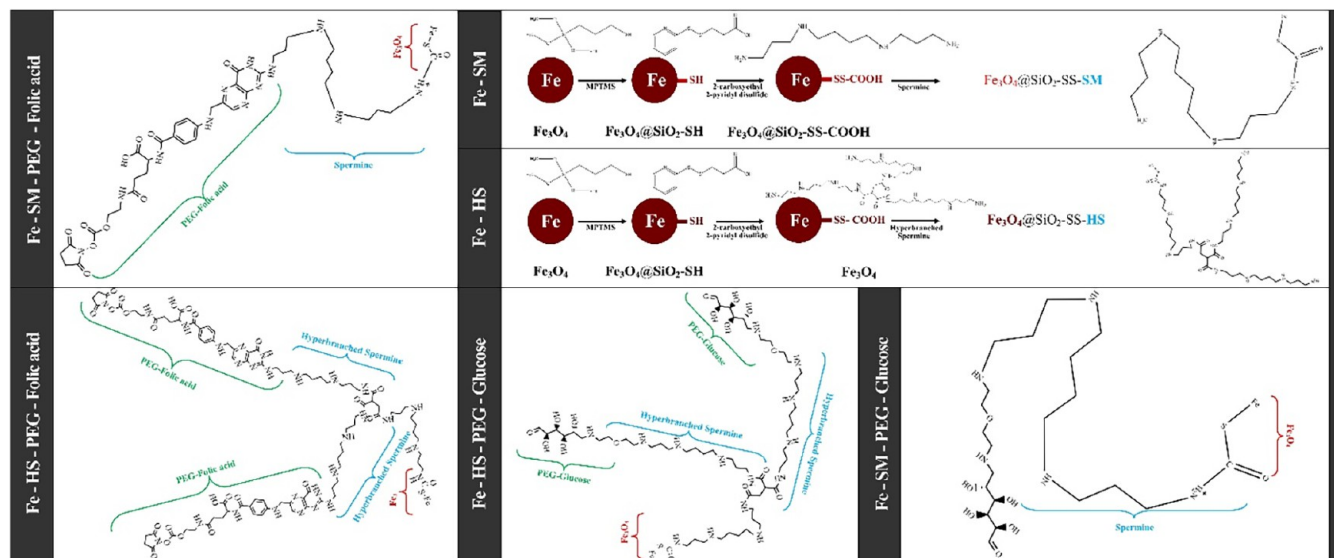


Figure 5. Schematic illustration of the synthesis of HS, FSM, FHS, FSMPF, FHSPF, FSMPG, and FHSPG NPs.

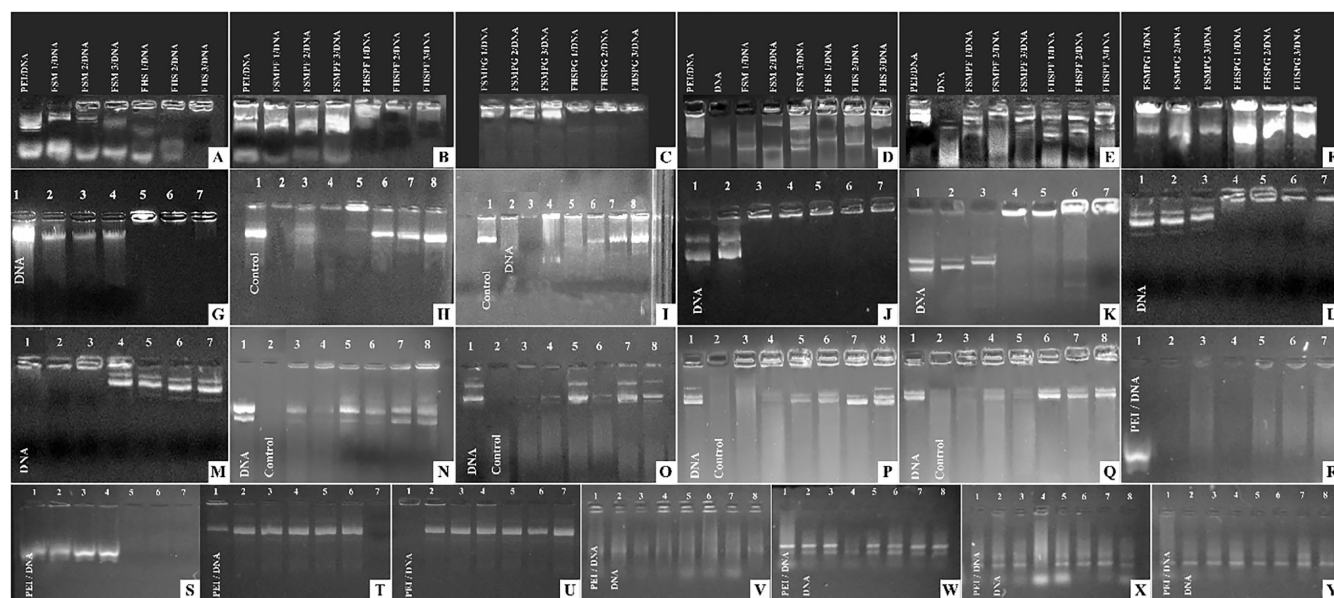


Figure 6. Retardation assay of MNPs (A–C). Agarose gel images of DNA extracted from the MNPs after enzyme treatment (D–F). By HSPG [1 = 5 μ g DNA; 2 = 5 μ g HSPG + 5 μ g DNA; 3 = 10 μ g HSPG + 5 μ g DNA; 4 = 25 μ g HSPG + 5 μ g DNA; 5 = 50 μ g HSPG + 5 μ g DNA; 6 = 100 μ g HSPG + 5 μ g DNA, and 7 = 200 μ g HSPG + 5 μ g DNA] (G); By HSPF [1 = 5 μ g DNA; 2 = 5 μ g HSPF + 5 μ g DNA; 3 = 10 μ g HSPF + 5 μ g DNA; 4 = 25 μ g HSPF + 5 μ g DNA; 5 = 50 μ g HSPF + 5 μ g DNA; 6 = 100 μ g HSPF + 5 μ g DNA; and 7 = 200 μ g HSPF + 5 μ g DNA] (H); and By HSPFG [1 = 5 μ g DNA; 2 = 2.5 μ g HSPF + 2.5 μ g HSPG + 5 μ g DNA; 3 = 5 μ g HSPF + 5 μ g HSPG + 5 μ g DNA; 4 = 10 μ g HSPF + 10 μ g HSPG + 5 μ g DNA; 5 = 25 μ g HSPF + 25 μ g HSPG + 5 μ g DNA; 6 = 50 μ g HSPF + 50 μ g HSPG + 5 μ g DNA; and 7 = 100 μ g HSPF + 100 μ g HSPG + 5 μ g DNA] (I). Protective effect of HS [1 = Control; 2 = 5 μ g DNA; 3 = 1 μ g HS + 5 μ g DNA; 4 = 2 μ g HS + 5 μ g DNA; 5 = 5 μ g HS + 5 μ g DNA; 6 = 10 μ g HS + 5 μ g DNA; 7 = 15 μ g HS + 5 μ g DNA; and 8 = 30 μ g HS + 5 μ g DNA] (J); By HSPG [1 = Control; 2 = 5 μ g DNA; 3 = 5 μ g HSPG + 5 μ g DNA; 4 = 10 μ g HSPG + 5 μ g DNA; 5 = 25 μ g HSPG + 5 μ g DNA; 6 = 50 μ g HSPG + 5 μ g DNA; 7 = 100 μ g HSPG + 5 μ g DNA; and 8 = 200 μ g HSPG + 5 μ g DNA] (K); By HSPF [1 = Control; 2 = 5 μ g DNA; 3 = 5 μ g HSPF + 5 μ g DNA; 4 = 10 μ g HSPF + 5 μ g DNA; 5 = 25 μ g HSPF + 5 μ g DNA; 6 = 50 μ g HSPF + 5 μ g DNA; 7 = 100 μ g HSPF + 5 μ g DNA; and 8 = 200 μ g HSPF + 5 μ g DNA] (L); By HSPFG [1 = Control; 2 = 5 μ g DNA; 3 = 2.5 μ g HSPF + 2.5 μ g HSPG + 5 μ g DNA; 4 = 5 μ g HSPF + 5 μ g HSPG + 5 μ g DNA; 5 = 10 μ g HSPF + 10 μ g HSPG + 5 μ g DNA; 6 = 25 μ g HSPF + 25 μ g HSPG + 5 μ g DNA; 7 = 50 μ g HSPF + 50 μ g HSPG + 5 μ g DNA; and 8 = 100 μ g HSPF + 100 μ g HSPG + 5 μ g DNA] (M) on DNA against plasma degradation; Retardation assay of (N and O) [1 = PEI/DNA; 2 = FSM1/DNA; 3 = FSM2/DNA; 4 = FSM3/DNA; 5 = FHS1/DNA; 6 = FHS2/DNA; 7 = FHS3/DNA], with along retardation assay of (P and Q) [1 = PEI/DNA; 2 = FSMPF1/DNA; 3 = FSMPF2/DNA; 4 = FSMPF3/DNA; 5 = FHSPF1/DNA; 6 = FHSPF2/DNA; 7 = FHSPF3/DNA] at different concentration of MNPs; Agarose gel images of DNA extracted from FSM3, FHS2, FSMPF1 and FHSPF2 NPs after enzyme treatment [1 = PEI/DNA; 2 = DNA; 3 = FSM1/DNA; 4 = FSM2/DNA; 5 = FSM3/DNA; 6 = FHS1/DNA; 7 = FHS2/DNA; 8 = FHS3/DNA] (R, S, T, L); And [1 = PEI/DNA; 2 = DNA; 3 = FSMPF1/DNA; 4 = FSMPF2/DNA; 5 = FSMPF3/DNA; 6 = FHSPF1/DNA; 7 = FHSPF2/DNA; 8 = FHSPF3/DNA] (V, W, X, Y); New figure prepared by the authors based on previously published data.^{2,12,35–37}

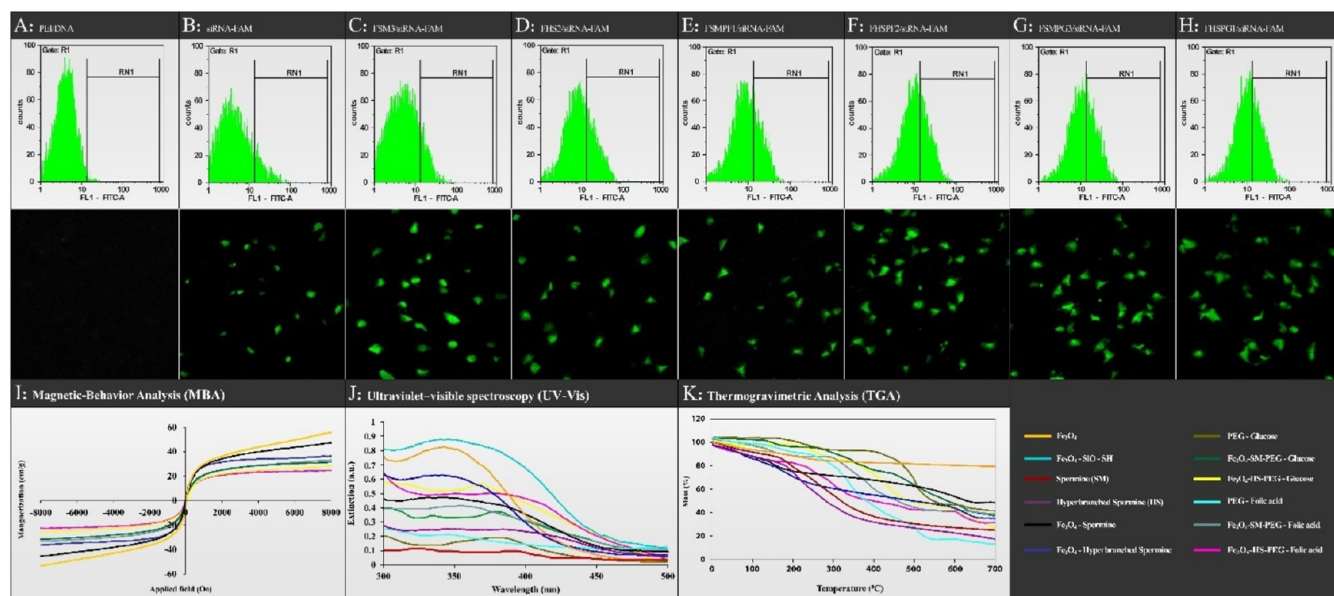


Figure 7. Flow cytometry “Up” and fluorescence “Down” (A–H) of MCF-7 cells, MBA (I), UV–vis (J), and TGA (K).

the structure of the synthesized NPs by EDX analysis. The structure of the synthesized NPs contains elements N, C, and O; this result is consistent with previous reports (Figure 4).^{2,12,28–31}

3.2. In Vitro Diagnostic Analysis of Our NPs. **3.2.1. In Vitro Cytotoxicity Assay Investigation of the Ability of FSM3, FHS2, FSMPF1, FHSPF2, FSMPG3, and FHSPG1 in Interaction and Protection of DNA against Enzymatic Digestion.** Figure 6 shows the analysis of the NPs structures with the concentrations that we selected. With increasing concentrations and types of NPs, the surface charge of DNA is neutralized and the DNA in the wells remains motionless. The results of agarose gel electrophoresis showed that all of the FHSPF, FSMPF, FHSPG, and FSMPG had a higher neutralization ability than PEI, FHS, or FSM in neutralizing the negative charge of DNA. As a result, the negative charge of DNA (5 g) was neutralized at 100 and 500 g concentrations of the FHSPF, FSMPF, FHSPG, and FSMPG NPs. Since FHSPF, FSMPF, FHSPG, and FSMPG NPs had noncationic NPs (PEG-FA or PEG-Glu), they may be less cationic than MNPs because they are coated with noncationic NPs. HS and SM NPs. Additionally, they contain high cationic amine groups that interact electrostatically with the negative charges of DNA's phosphate groups, thereby neutralizing them. When high ratios of nanovectors to DNA are present in the agarose gel, DNA movement is reduced toward the positive pole of the device. For this reason, higher concentrations of FSM and FHS NPs are needed more than those of FHSPF, FSMPF, FHSPG, and FSMPG NPs to neutralize the negative charge on DNA. The observed absence of the PEI/DNA band in the retardation assay is likely due to excessive DNA condensation resulting from PEI's high positive charge, which hinders gel migration. Large aggregate formation and potential DNA degradation at high PEI concentrations may also contribute. Sample preparation errors, such as improper ratios or mixing, represent further possible causes for this result (Figure 6). In this study, NPs were investigated for their ability to protect DNA from restriction enzymes. The intricate structure of our NPs is vividly illustrated in Figure 5. This graphic depiction clearly highlights the spatial arrangement of distinct charge regions

and unique dipole moments exhibiting a sponge-like architecture. This configuration arises from the alternating linkage of glucose, folic acid, iron, and both mono- and branched spermines as well as PEG chains. Such a design highlights the multifunctional surface chemistry and complex electrostatic landscape of the NPs, which explains their interaction behavior with DNA, a negatively charged biomolecule.²⁸

The cell's defense mechanism destroys more than 99% of DNA transferred via the endocytosis-dependent pathway. The ability of the NPs to protect DNA from the restriction enzymes is therefore essential. Based on the results of our study, the NPs are more effective in protecting DNA against restriction enzymes when they are more concentrated. This is clearly evident in Figure 6, where no bands of DNA were observed in the well of control DNA treated with DNase I, indicating that the enzyme had destroyed it. At concentrations of 100 or 500 μ g, FHS and FSM nanoparticles did not protect DNA from the restriction enzymes. When the concentration of the NPs was increased to 1000 g, the resolution of agarose gel bands gradually improved. The NPs containing FSM/DNA did not degrade compared to the control at concentrations of up to 1000 g. Furthermore, the NPs containing FHSPF, FSMPF, FHSPG, and FSMPG NPs proved to be highly effective in preventing DNA degradation against the restriction enzymes. To evaluate optimal concentrations, we first tested FSM and FHS nanoparticles in guar cell suspension cultures to establish an effective range. Beyond the findings in Figure 6, we also thoroughly examined the interactions of the individual components of our iron-based nanoparticles throughout this study. These analyses covered single-component configurations, binary conjugations with spermine or hyperbranched spermine, and ternary complexes incorporating folic acid, PEG, or glucose. The progression and configuration of these complexes are documented in the figure captions. All related results have been published across multiple peer-reviewed articles, and their accuracy and reproducibility have been confirmed. Considering the four-year duration of this project and the stepwise optimization at each stage, this section synthesizes the key functional interactions between our

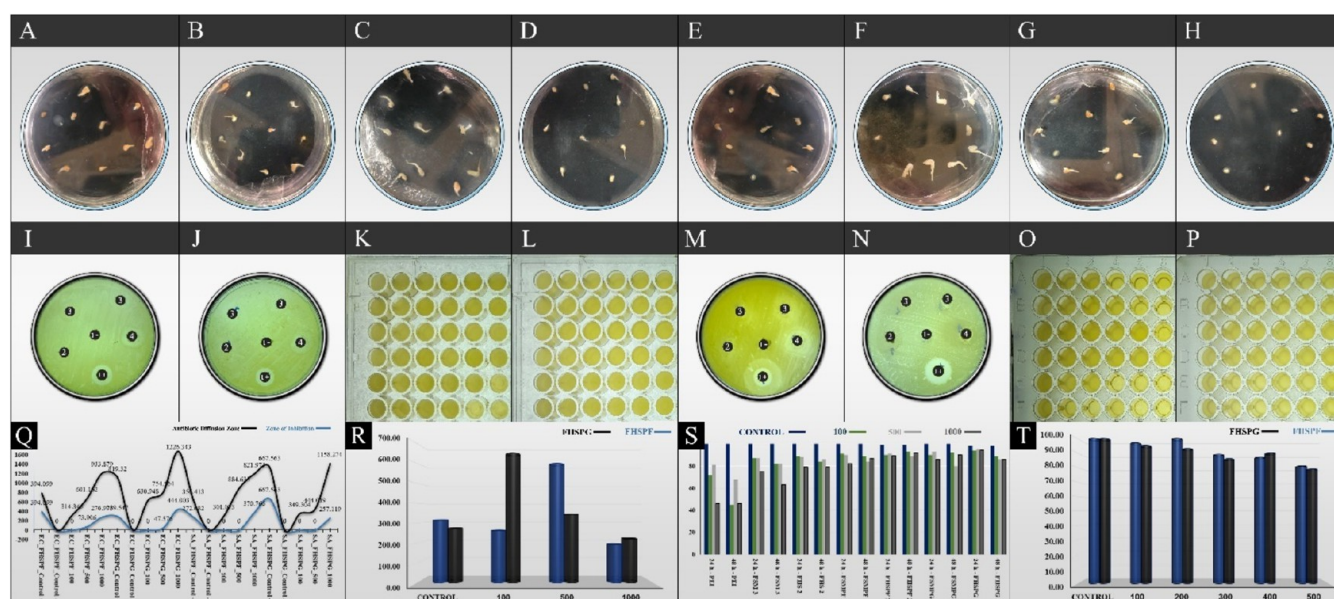


Figure 8. Petri dish images showing Guar callus treated with FHSPF2 NPs at concentrations of 0 (A), 100 (B), 500 (C), and 1000 $\mu\text{g/mL}$ (D). Petri dish images showing Guar callus treated with FHSPG1 NPs at concentrations of 0 (E), 100 (F), 500 (G), and 1000 $\mu\text{g/mL}$ (H). (I) Disk diffusion assay images demonstrating the antibacterial activity of FHSPF2 NPs against *E. coli* at positive control (1+), negative control (1-), 100 $\mu\text{g/mL}$ (2), 500 $\mu\text{g/mL}$ (3), and 1000 $\mu\text{g/mL}$ (4). (J) Disk diffusion assay images showing the antibacterial activity of FHSPF2 NPs against *S. aureus* at positive control (1+), negative control (1-), 100 $\mu\text{g/mL}$ (2), 500 $\mu\text{g/mL}$ (3), and 1000 $\mu\text{g/mL}$ (4). (K) MIC test images illustrating antibacterial activity of FHSPF2 NPs against *S. aureus* at concentrations 0, 100, 250, and 500 $\mu\text{g/mL}$. (L) MIC test images illustrating antibacterial activity of FHSPF2 NPs against *E. coli* at concentrations 0, 100, 250, and 500 $\mu\text{g/mL}$. (M) Disk diffusion assay images demonstrating antibacterial activity of FHSPG1 NPs against *E. coli* at positive control (1+), negative control (1-), 100 $\mu\text{g/mL}$ (2), 500 $\mu\text{g/mL}$ (3), and 1000 $\mu\text{g/mL}$ (4). (N) Disk diffusion assay images showing antibacterial activity of FHSPG1 NPs against *S. aureus* at positive control (1+), negative control (1-), 100 $\mu\text{g/mL}$ (2), 500 $\mu\text{g/mL}$ (3), and 1000 $\mu\text{g/mL}$ (4). (O) MIC test images illustrating antibacterial activity of FHSPG1 NPs against *S. aureus* at concentrations 0, 100, 250, and 500 $\mu\text{g/mL}$. (P) MIC test images illustrating antibacterial activity of FHSPG1 NPs against *E. coli* at concentrations 0, 100, 250, and 500 $\mu\text{g/mL}$. (Q) Graph depicting inhibition zone diameters (blue) and dispersion zone diameters (black) from disk diffusion assays of the NPs, analyzed using ImageJ software. (R) Graph showing the ratio of callus volume to total Petri dish area for FHSPG1 and FHSPF2 NPs, analyzed by ImageJ software. (S) Chart showing cell viability assessment for all NPs tested on an animal cell model. (T) Comparison of the average effects of FHSPG1 and FHSPF2 NPs on the viability of Guar cells.

nanoparticles and DNA. To facilitate accessibility for readers, these findings have been systematically compiled in one place. This section serves as a synthesis of the structural and functional insights gained in this project, providing a practical reference for future studies.^{21,23,24,28,32–34}

Our study demonstrates the effectiveness of the developed NPs in delivering DNA to MCF-7 cells. FSMPF1, FHSPF2, FSMPG3, and FHSPG1 showed significantly higher transfection efficiency compared to those of FSM3, FHS2, and the PEI/DNA complex. Surface modifications with spermine, PEG, folic acid, and glucose appear to enhance the cellular uptake and gene expression. PEG likely reduces nonspecific serum interactions and prevents aggregation, contributing to the stability of NPs, as supported by previous research. Fluorescence microscopy and flow cytometry confirmed that these NPs successfully entered cells and released intact DNA. The presence of folate moieties may facilitate receptor-mediated uptake, which is particularly relevant in folate receptor-overexpressing cancer cells. Moreover, the use of hyperbranched spermine and PEG likely protects DNA from enzymatic degradation, which is essential for efficient gene transfer. Overall, FSMPF1, FHSPF2, FSMPG3, and FHSPG1 are promising nonviral vectors, offering efficient delivery, sustained gene expression, and enhanced DNA protection. These findings support their potential for future applications in cancer gene therapy. These findings are consistent with recent studies demonstrating that surface modification of NPs with

spermine and folic acid significantly enhances gene delivery efficiency and targeted uptake in folate receptor-overexpressing cancer cells. At the same time, PEG improves the stability of NPs and protects DNA from enzymatic degradation (Figure 7).^{38,39}

To evaluate the cytotoxic effects of FHSPF2 and FHSPG1 NPs on Guar cells, a two-phase experiment was conducted using a suspension culture system derived from nodal callus tissue. In the first phase, cells were treated with concentrations of 0, 100, 500, and 1000 $\mu\text{g/mL}$ of both NPs. The results revealed no significant cytotoxicity up to 500 $\mu\text{g/mL}$, with cell viability consistently exceeding 80%. At 1000 $\mu\text{g/mL}$, a slight reduction in the viability was observed, suggesting a possible concentration-dependent response at high levels. Based on these preliminary results, the second phase was designed to assess finer concentration intervals (0, 100, 200, 300, 400, and 500 $\mu\text{g/mL}$). Cell viability was determined using the trypan blue exclusion assay, with viable and nonviable cells counted microscopically. Across all tested concentrations in both FHSPF2- and FHSPG1-treated groups, viability remained above 80%, indicating low toxicity and confirming the threshold identified in Phase one. The viability of Guar cells treated with various concentrations of FHSPF2 and FHSPG1 NPs remained above 80%, indicating minimal cytotoxicity compared with the untreated control group. This suggests that the NPs, composed of Fe_3O_4 , spermine, PEG, folic acid, and glucose, exhibit favorable biocompatibility with plant cells.

Table 1. Analysis of Variance of the Morphological and Physiological Parameters of *Guar* under the Influence of Our NPs and CuO Stress

SOV	Df	mean squares							
		TDW	TL	RV	NL	SES	SEP	RWC	OP
nanoparticles (NP _s)	6	0.00036 ^a	545.09 ^a	5.79 ^a	25.98 ^a	0.13 ^a	2316.50 ^a	1479.19 ^a	5.52 ^a
CuO stress (CS)	1	0.00017 ^a	257.57 ^a	0.70 ^a	1.89 ^a	0.02 ^a	786.37 ^a	508.93 ^a	2.52 ^a
NP _s * CS	6	0.00001 ^a	4.77 ^a	0.11 ^{ns}	0.10 ^{ns}	0.001 ^a	81.12 ^a	46.37 ^a	0.18 ^{ns}
error	28	0.0000003	0.30	0.05	0.11	0.0004	0.24	1.22	0.09
CV		2.05	2.46	10.53	8.00	3.04	0.63	1.49	10.49

^aSignificant at 1% probability level; ns, not significant.

Figure 8T illustrates this compatibility. Visual observations of *Guar* callus morphology are provided for the control (Figure 8A), 100 $\mu\text{g}/\text{mL}$ (Figure 8B), 500 $\mu\text{g}/\text{mL}$ (Figure 8C), and 1000 $\mu\text{g}/\text{mL}$ treatments (Figure 8D) to FHSPF2 and also the control (Figure 8E), 100 $\mu\text{g}/\text{mL}$ (Figure 8F), 500 $\mu\text{g}/\text{mL}$ (Figure 8G), and 1000 $\mu\text{g}/\text{mL}$ treatments (Figure 8H) to FHSPG1. Even at higher concentrations, NPs did not cause significant cellular damage. These findings confirm the suitability of FHSPF2 and FHSPG1 for potential biotechnological applications in plant systems. The structural integrity and metabolic activity of the callus tissue were maintained. Overall, the formulations appeared safe for use in plant cell experiments. To enhance the quantitative and qualitative reliability of our findings, we employed advanced image processing techniques, using ImageJ software. This allowed us to precisely measure callus size and its expansion relative to the Petri dish surface, offering a clear and objective visualization of NPs' biocompatibility with plant cells (Figure 8R). The biocompatibility of FHSPF2 and FHSPG1 NPs with *Guar* cells aligns with recent studies. For instance, Kolokithas-Ntoukas et al. (2025) reported that PEG-coated iron oxide NPs exhibited no cytotoxicity in NIH/3T3 cells even at concentrations up to 500 $\mu\text{g}/\text{mL}$, maintaining approximately 100% cell viability.⁴⁰ Additionally, Afrouz et al. demonstrated that hyperbranched spermine-based nanoparticles, functionalized with PEG and folic acid, showed high biocompatibility in both in vitro and in vivo models, supporting their potential in gene delivery applications.²⁸

The cytotoxicity of FSM3, FHS2, FSMPF1, FHSPF2, FSMPG3, and FHSPG1 NPs was evaluated on MCF-7 human breast cancer cells using the MTT assay after 24 and 48 h of exposure at concentrations of 0, 100, 500, and 1000 $\mu\text{g}/\text{mL}$. PEI, a known cytotoxic gene delivery vector, served as a reference control. The findings demonstrated that FSMPF1, FHSPF2, FSMPG3, and FHSPG1 NPs maintained high cellular viability, consistently exceeding 85% at concentrations up to 1000 $\mu\text{g}/\text{mL}$ after 24 h, indicating excellent biocompatibility. Conversely, FSM3 and FHS2 NPs exhibited moderate cytotoxic effects, particularly at higher doses. Specifically, cell viability after 24 h at 100 $\mu\text{g}/\text{mL}$ was reduced to 42.3% for PEI, compared to 84.9 and 86.7% for FSM3 and FHS2, respectively. Notably, even at 1000 $\mu\text{g}/\text{mL}$, FHSPF2 and FHSPG1 preserved cell viability at 89.72 and 92.01%, respectively, whereas PEI led to a marked decline in viability (38.8% at 72 h). These results highlight the superior safety profile of FHSPF2 and FHSPG1, likely due to their functionalization with biocompatible moieties such as spermine, PEG, folic acid, and glucose (Figure 8S). The high biocompatibility of FHSPF2 and FHSPG1 NPs with MCF-7 cells is consistent with the recent research findings. A 2024 study published in ACS Omega demonstrated that folic acid-

functionalized, PEGylated magnetic NPs effectively targeted folate receptor-overexpressing tumor cells, enhancing therapeutic delivery while maintaining minimal cytotoxicity.³⁹ Similarly, research in Cancer Nanotechnology reported that PEGylated nanosomes functionalized with folic acid exhibited enhanced anticancer efficacy and reduced toxicity in breast cancer cells.⁴¹

Antibacterial testing further supported the low-toxicity profile of these formulations. At 1000 $\mu\text{g}/\text{mL}$, FSMPG3 and FHSPG1 displayed only mild antibacterial activity compared with the tetracycline control, whereas the 500 $\mu\text{g}/\text{mL}$ concentration showed minimal inhibition, indicating a low antimicrobial impact. This concentration thus appears to be optimal, as it balances structural stability with biological safety. As shown in Figure 8, the NPs exhibited a highly uniform dispersion, supporting their controlled-release potential and efficient interaction with biological tissues. Notably, the minimal effect on microbial viability at 500 $\mu\text{g}/\text{mL}$ suggests that these NPs are unlikely to disrupt beneficial microorganisms such as symbiotic bacteria, fungi, or nematodes. For ease of validation, we performed image analysis using ImageJ software, where we quantitatively assessed callus size and growth relative to the Petri dish surface as an objective metric (Figure 8, image Q). For antibacterial testing, we evaluated concentrations up to 500 $\mu\text{g}/\text{mL}$. The MIC assessment, based on visual inspection, showed no observable color change, and MBC analysis further confirmed the absence of bactericidal activity. Growth of both Gram-positive and Gram-negative bacterial colonies proceeded without disruption, indicating that these NPs do not hinder beneficial microbial populations. Together, these findings reinforce the excellent biocompatibility and safety profile of FSMPF1, FHSPF2, FSMPG3, and FHSPG1 NPs for biomedical and biotechnological uses. Recent studies support our findings on the biocompatibility and low antimicrobial impact of functionalized NPs. A 2025 study in Nature Communications demonstrated that stomata-targeted nanocarriers enhanced plant defense without disrupting beneficial microorganisms, aligning with our observations of minimal microbial disturbance.⁴² Additionally, a 2024 ACS Omega article reported that metal-doped iron oxide NPs exhibit low antibacterial activity at therapeutic doses, reinforcing the safety profile of FSMPG3 and FHSPG1.⁴³ Together, these studies confirm the potential of these nanoparticles for safe use in biomedical and agricultural applications.

In conclusion, the cytotoxicity and antibacterial results highlight the excellent biocompatibility of the FSMPF1, FHSPF2, FSMPG3, and FHSPG1 nanoparticles. Their low toxicity toward mammalian cells and minimal effects on microbial systems make them strong candidates for biomedical and biotechnological applications, particularly for gene delivery

Table 2. Means Comparison of the Morphological and Physiological Parameters of *Guar* under the Influence of Our NPs and CuO Stress¹

	treatments	TDW gr	TL cm	RV number	NL	SES	SEP	RWC	OP
normal-irrigation	control	0.023 ^g	11.62 ^k	0.97 ^{ef}	1.85 ^g	0.51 ^g	59.12 ^l	58.82 ^h	2.25 ^f
	FSM	0.024 ^f	19.17 ^h	1.95 ^d	2.92 ^f	0.58 ^f	70.98 ⁱ	70.86 ^{ef}	2.87 ^{de}
	FHS	0.026 ^e	21.75 ^g	1.97 ^d	4.12 ^{de}	0.66 ^e	75.06 ^h	72.90 ^e	2.65 ^{ef}
	FSMPF	0.031 ^c	26.90 ^e	2.55 ^{bc}	4.45 ^{de}	0.65 ^e	87.64 ^e	76.30 ^d	2.55 ^{ef}
	FHSPF	0.032 ^c	28.90 ^d	2.75 ^{bc}	5.20 ^{bc}	0.74 ^{cd}	90.03 ^d	81.42 ^c	3.47 ^{bc}
	FSMPG	0.035 ^b	30.70 ^c	2.97 ^{ab}	5.52 ^b	0.80 ^{ab}	94.90 ^b	87.58 ^b	4.02 ^{ab}
	FHSPG	0.037 ^a	33.27 ^a	3.30 ^a	7.22 ^a	0.83 ^a	96.91 ^a	92.45 ^a	4.10 ^a
CuO stress	control	0.15 ⁱ	5.27 ^l	0.65 ^f	1.47 ^g	0.43 ^h	39.96 ^m	45.90 ⁱ	1.32 ^g
	FSM	0.018 ^h	13.87 ^j	1.30 ^e	2.72 ^f	0.52 ^g	60.89 ^k	60.48 ^h	2.30 ^{ef}
	FHS	0.023 ^g	16.95 ⁱ	1.92 ^d	3.35 ^f	0.59 ^f	67.23 ^j	65.35 ^g	2.22 ^f
	FSMPF	0.027 ^{de}	22.50 ^g	2.35 ^{cd}	4.05 ^e	0.63 ^e	78.61 ^g	70.30 ^f	2.27 ^f
	FHSPF	0.028 ^d	24.77 ^f	2.47 ^c	4.75 ^{cd}	0.72 ^d	85.33 ^f	76.61 ^d	3.30 ^{cd}
	FSMPG	0.034 ^b	27.05 ^e	2.77 ^{bc}	5.17 ^{bc}	0.78 ^{bc}	93.37 ^c	86.18 ^b	3.42 ^{cd}
	FHSPG	0.038 ^a	31.87 ^b	3.42 ^a	7.20 ^a	0.82 ^a	96.80 ^a	93.31 ^a	4.10 ^a

¹Means in each column followed by a similar letter(s) are not significantly different at 1% probability level, using the LSD test.

and tissue engineering, where safety and functional integration are critical.^{2,12,29–31}

3.3. Effect of CuO Stress and Our NPs Application on *Guar*. 3.3.1. *Effect of CuO Stress and Our NPs Application on the Morphological and Physiological Parameters of *Guar*.* The effects of the FSM3, FHS2, FSMPF1, FHSPF2, FSMPG3, and FHSPG1 NPs treatments on TDW, TL, RV, NL, SES, SEP, RWC, and OP of *Guar* were dependent on NPs and culture medium type and are summarized in Table 1.

3.3.2. *Guar Morphological and Physiological Responses to Our NPs.* This study showed that coatings with FSM3, FHS2, FSMPF1, FHSPF2, FSMPG3, and FHSPG1 positively influenced TDW, TL, RV, NL, SES, SEP, RWC, and OP. In both culture media (with and without CuO stress), the application of our nanoparticles improved the morphological and physiological traits of *guar* compared to the control. Analysis of variance showed that the interaction between NPs and CuO stress (NPs × CS) significantly affected TDW, TL, SEP, and RWC (Tables 1 and 2). Among the treatments, multibranch polyamines enhanced plant growth more effectively than single-branched polyamines. These results also showed high utilization efficiency of FSMPG3 and FHSPG1 compared to those of FSMPF1 and FHSPF2, respectively. Additionally, FHSPG1 and FHSPF2 demonstrated higher efficiency compared to FSMPG3 and FSMPF1, respectively. This greater efficiency was observed in both culture media with and without CuO stress. The increase in efficiency compared to the control, FSM3, and FHS2 treatments in FSMPF1, FHSPF2, FSMPG3, and FHSPG1, as multibranch polyamines, indicates the significant ability of these NPs to enhance the morphological and physiological parameters of *Guar*. In other words, FSMPG3 and FHSPG1 increased the speed of seedling establishment and germination uniformity in both culture media, likely due to enhanced metabolic activity in the seeds. The increase in seedling establishment (SES and SEP) with the application of FSMPF1, FHSPF2, FSMPG3, and FHSPG1 NPs is most likely due to an increase in protein synthesis in seeds, along with an increase in the availability of glucose and folic acid, which optimize positive metabolic activities in *Guar* seedlings. Moreover, the increase in SES may result from faster water absorption and activation of hydrolytic enzymes, which accelerate germination and radicle growth. Thus, FSMPF1, FHSPF2, FSMPG3, and

FHSPG1 nanoparticles positively affected seedling establishment and improved the morphological and physiological parameters (TDW, TL, RV, NL, SES, SEP, RWC, and OP) of *guar* under CuO stress.

During heightened metabolic activity, proteins and nucleic acids are synthesized, hydrolytic enzymes are activated, stored nutrients are mobilized to the embryonic axis, and cellular repair and regeneration begin. These processes led to increased seedling growth, TDW, and TL. The application of single-branched and conjugated PAs on *Brassica napus* was reported to increase seedling growth rates. This research confirms that micronutrients, such as iron NPs, increase TDW and TL when used in sorghum seeds.⁴⁴ Plants utilize polyamines (such as spermine), glucose, and folic acid to support a wide range of physiological processes, including seed germination, shoot and root development, water uptake, and overall biomass accumulation.^{2,12,22,27,45,46} In addition to metabolic activation and organellar structure biogenesis, stored foods (substances) are mobilized, and cells are elongated, replicated, and divided during seed germination. According to previous studies, PA concentration increases during germination in rice.⁴⁷

Spermine application increases seed germination, water absorption, and plant volume in *Vigna radiata*.⁴⁸ The endosperm is compressed during priming as the embryo develops.⁴⁹ As a result of the endosperm cell walls' hydrolytic activity, the primed seed may absorb water more quickly and germinate faster. PAs, however, enhanced both the RWC and OP in our study. In the early stages of seedling growth, this is crucial for the development of shoots and roots, water absorption, and overall plant volume increase. Researchers have found that PAs enhance gene regeneration, resulting in improved TDW, TL, RV, and NL. *Hordeum jubatum* germination, growth, germination percentage, TDW, TL, RV, NL, and plant protection have been shown to be improved by PAs.⁵⁰ Our current study confirmed these results. The polycationic nature of SM and HS (as polyamines), along with PEG, glucose, and folic acid, can therefore be confirmed.

The amino and imino groups form hydrogen and ionic bonds with negatively charged nucleic acids, proteins, and phospholipids, thereby contributing to zygote polarity establishment, apical axis formation, cell layer differentiation, and meristem development.⁵¹ With exogenous PAs (our SM or HS) and PAs synthesis inhibitors, nucleic acid synthesis (by

Table 3. Analysis of Variance of the Antioxidant Defense (Antioxidant Enzyme Activity) and Oxidative Damage of *Guar* under the Influence of Our NPs and CuO Stress

SOV	Df	mean squares					
		ANC	PPO	POX	CAT	H ₂ O ₂	PRL
nanoparticles (NP _s)	6	118.31 ^a	595.44 ^a	588.97 ^a	345.94 ^a	0.77 ^a	1.69 ^a
CuO stress (CS)	1	145.89 ^a	2026.94 ^a	1906.56 ^a	1416.59 ^a	11.38 ^a	10.67 ^a
NP _s * CS	6	1.83 ^a	13.88 ^a	36.32 ^a	111.18 ^a	0.15 ^a	0.29 ^a
error	28	0.14	0.24	0.12	0.68	0.0006	0.003
CV		2.60	0.93	1.22	3.43	1.14	2.74

^aSignificant at 1% probability level; ns, not significant.

folic acid) and protein translation (by glucose) can be regulated in both directions. In addition to affecting the development of organelles such as the endoplasmic reticulum, mitochondria, and plastids, it also affects the structure of microtubules. Several endogenous hormones are essential for somatic embryogenesis and plantlet development including IAA, cytokinins, ethylene, ABA, and PAs. Plant tissues and cell cultures have demonstrated that PAs play a crucial role in inducing cell division and promoting regeneration (Tables 1 and 2). Consequently, TDW, TL, RV, NL, SES, SEP, RWC, and OP increased.^{12,14,22,51} Environmental stress reduces nutrient availability and uptake, thereby limiting the production of secondary metabolites. In this study, the application of FSMPG3, FHSPG1, and other PAs-based NPs enhanced Fe and N absorption, improved root structure by increasing the number of thin, hairy roots, and promoted secondary metabolite synthesis. Spermine, PEG, glucose, and folic acid in the coatings facilitated nutrient mobilization, activated antioxidant defense, and enhanced gene expression, collectively boosting plant resilience under CuO stress. Consequently, treated *Guar* plants exhibited higher nutrient content, stronger antioxidant responses, and improved growth compared with untreated controls. These results demonstrate that multifunctional NPs can mitigate heavy metal stress while enhancing the overall plant health and productivity.

3.3.3. Effect of CuO Stress and Our NPs Application on Antioxidant Defense (Antioxidant Enzyme Activity) or Oxidative Damage of *Guar*. The effects of the FSM3, FHS2, FSMPF1, FHSPF2, FSMPG3, and FHSPG1 treatments on ANC, PPO, POX, CAT, H₂O₂, and PRL of *Guar* were NP and culture medium type dependent, and are summarized in Table 3. The data show that the treatment had a significant effect on all parameters.

3.3.4. Effects of NPs on Antioxidant Defense or Oxidative Damage of *Guar*. Antioxidant enzyme activity, as an indicator of stress, was more evident in *Guar* subjected to CuO stress compared with the controls, resulting in significant increases in ANC, PPO, POX, CAT, H₂O₂, and PRL activities in the heavy-metal-stressed plants. Indeed, copper contributes to the defense mechanism; however, chronic Cu toxicity can lead to severe poisoning and oxidative damage. Hence, changing specific antioxidant enzymes' activities as a result of oxidative stress conditions. The present study showed that the application of coatings of FSM3, FHS2, FSMPF1, FHSPF2, FSMPG3, and FHSPG1 had a positive effect on ANC, PPO, POX, CAT, and PRL, along with a negative effect on H₂O₂.

On the other hand, the results showed that in two types of culture medium (with and without CuO stress), the application of our NPs had a positive effect on the characteristics of antioxidant defense or oxidative damage in *Guar* compared to the control treatment. In other words, the

highest content of antioxidant defense or oxidative damage was documented for FHSPG1 NPs treatment in two types of culture medium (with and without CuO Stress). Multi-branched PAs were found to increase plant productivity compared to single-branched PAs. Notably, these results demonstrate the high utilization efficiency of FHSPG1 compared to FSMPG3 and FHSPG1 compared to FHSPF2. This increase in efficiency was observed in both culture media with and without CuO stress. The increase in efficiency of FSM3 and FHS2 treatment in FSMPF1, FHSPF2, FSMPG3, and FHSPG1 in multibranched PAs over the control indicates the significant ability of these NPs to increase the antioxidant defense or oxidative damage of *Guar*.^{2,12,27,45,46}

As a result of CuO stress, *Guar* plants produce reactive oxygen species (ROS), which cause oxidative stress. In the presence of environmental stresses, our NPs maintain redox equilibrium by scavenging excessive ROS. Heavy metal stress may cause an oxidative burst. Consequently, excess copper activated antioxidant enzyme genes in crops, including SOD, POD, and CAT, which facilitate the removal of reactive oxygen species (ROS).¹ A significant increase in APX and POD has been observed in *Brassica napus* roots and leaves after excessive copper exposure.⁵² Consequently, ROS caused by copper exposure is scavenged in this study by increasing the peroxidase activity. As a result of the use of iron, SM or HS (as PAs), PEG, glucose, and folic acid, the antioxidant enzyme activity was increased.

As most cell parts can produce reactive oxygen species as a result of stress, this research could strengthen the plant's defense system by applying our treatments. Hydrogen peroxide neutralizes enzymes that include iron, catalase, and peroxidase, which are among the most significant for plant activity. The activities of these enzymes may be affected by iron deficiency. This is why an iron deficiency can cause chlorosis in plants as well as inhibit a few enzymes, including catalase and peroxidase. These enzymes serve a unique function in plant metabolism when iron porphyrins are present. SM and glucose are plant defenses against oxidative stress that induce the production of more endogenous PAs under stress. Externally applied SM has been shown to increase the PAs levels in thylakoid membranes. Studies have shown that spermine can quench singlet oxygen and act as a free radical scavenger, thereby protecting DNA from damage caused by reactive oxygen species (ROS).⁵³ Studies indicate that the plant plasma membrane is the primary target of heavy metal toxicity, and because spermine mitigates oxidative damage, it can protect the membrane from free radical-induced injury.⁵⁴ Our findings are consistent with previous studies, which show that polyamines, iron (Fe₂O₃), spermine or homospermine (as polyamines), PEG, glucose, and folic acid are associated with

Table 4. Means Comparison of the Antioxidant Defense (Antioxidant Enzyme Activity) and Oxidative Damage of *Guar* under the Influence of Our NPs and CuO Stress^a

	treatments	ANC OD $\mu\text{g Pro min}^{-1}$	PPO OD $\mu\text{g Pro min}^{-1}$	POX OD $\mu\text{g Pro min}^{-1}$	CAT OD $\mu\text{g Pro min}^{-1}$	H ₂ O ₂ $\mu\text{mol/g FW}$	PRL $\mu\text{g/g Fw}$
normal-irrigation	control	6.48 ^l	31.72 ^m	7.06 ^j	11.02 ⁱ	2.04 ^g	1.09 ^l
	FSM	11.18 ^h	43.32 ^l	17.69 ⁱ	16.47 ^h	2.93 ^b	1.72 ^{ij}
	FHS	12.36 ^g	45.03 ^k	22.99 ^h	20.31 ^g	3.15 ^a	1.67 ^j
	FSMPF	13.45 ^f	51.40 ⁱ	28.39 ^f	25.50 ^d	2.74 ^c	1.33 ^k
	FHSPF	14.60 ^e	48.11 ^j	32.91 ^e	20.42 ^{fg}	2.72 ^c	1.83 ^{hi}
	FSMPG	16.83 ^{cd}	55.39 ^f	27.85 ^f	21.93 ^{ef}	2.43 ^d	2.13 ^g
	FHSPG	17.23 ^{cd}	54.37 ^g	23.37 ^h	17.63 ^h	2.35 ^e	1.94 ^h
CuO stress	control	8.24 ⁱ	43.26 ^l	18.00 ⁱ	12.24 ⁱ	1.34 ^l	1.33 ^k
	FSM	14.55 ^e	52.38 ^h	27.16 ^g	22.40 ^e	2.13 ^f	2.33 ^f
	FHS	16.69 ^d	56.58 ^e	33.21 ^e	26.72 ^d	1.96 ^h	2.46 ^e
	FSMPF	17.45 ^c	60.50 ^d	38.76 ^d	31.66 ^c	1.86 ⁱ	2.71 ^d
	FHSPF	18.27 ^b	62.90 ^c	39.79 ^c	32.71 ^c	1.34 ^l	2.84 ^c
	FSMPG	18.92 ^b	67.53 ^b	41.44 ^b	36.75 ^b	1.68 ^k	2.96 ^b
	FHSPG	20.61 ^a	70.41 ^a	43.60 ^a	41.19 ^a	1.75 ^j	3.17 ^a

^aMeans in each column followed by a similar letter(s) are not significantly different at 1% probability level, using the LSD test.

Table 5. Analysis of Variance of the Secondary Metabolites and Content of Elements of *Guar* under the Influence of Our NPs and CuO Stress

SOV	Df	mean squares					
	Df	N	Fe	α -pinene	α -terpinene	camphene	1,8-cineol
nanoparticles (NP _s)	6	4.65 ^a	2.22 ^a	31.13 ^a	327.58 ^a	2.22 ^a	9.37 ^a
CuO stress (CS)	1	6.85 ^a	3.20 ^a	0.09 ^{ns}	161.36 ^a	3.30 ^a	11.65 ^a
NP _s * CS	6	0.12 ^a	0.12 ^a	1.92 ^a	14.89 ^a	0.13 ^a	0.21 ^{ns}
error	28	0.02	0.0009	0.08	1.43	0.002	0.15
CV		4.67	1.33	2.41	3.57	1.94	10.98

^aSignificant at 1% level of probability; ns not significant.

enhanced antioxidant enzyme activity under stress conditions.^{2,12,27,45,46}

According to a previous study,⁵⁵ PAs regulate redox homeostasis in plants, which plays a dual or complex role in oxidative stress (Cd and Cu have frequently been implicated in fluctuations in the scavenging system in cells). The phytoalexins found in plants can increase the activity of antioxidant enzymes, thereby regulating oxidative stress caused by various environmental factors in plants. As a result of exposure to cadmium and copper, lipid peroxidation increased in sunflower leaf discs, whereas glutathione reductase (GR) and superoxide dismutase (SOD) activities decreased.⁵⁶ Plants treated with exogenous PAs (1 mM) had their lipid peroxidation effects reduced almost to control levels with the SM treatment. Furthermore, the SM treatment completely restored GR activity, and it also completely restored SOD activity under Cu²⁺ treatment. PAs produce reactive oxygen species. However, during times of stress, PAs can cause cell damage due to their catabolism of H₂O₂ and acrolein.⁵⁷

As a signaling molecule, H₂O₂ can enter the stress signal transduction chain and activate an antioxidant defense response. In particular, hydrogen peroxidase accumulation seems to be a critical event causing growth reduction.⁵⁸ A possible explanation for the increase in H₂O₂ levels after exposure to Ni was provided. The mechanisms by which metals induce ROS in crops depend on their chemical properties. There are also mechanisms by which metals induce ROS production. As a result of NPs being supplied, H₂O₂ levels were reduced to minimum and maximum levels for FHSPG1 and the control. Accordingly, it is shown that coating

Fe₃O₄ NPs with SM or HS (as PAs), PEG, glucose, and folic acid decreases hydrogen peroxide by increasing the activity of enzymes in the oxidative defense system, such as catalase and peroxidase, and thus reduces hydrogen peroxide.

Our results suggested that NPs enhanced cell membrane stability and permeability by acting as scavengers against H₂O₂ and O₂. *Guar* plants have been shown to respond to NPs in different ways, such as by scavenging ROS triggered by NPs, thereby reducing their harmful effects (Tables 3 and 4). We found that the application of culture medium with heavy metals (with and without CuO stress) led to reduced morphological and physiological parameters as well as decreased antioxidant defense (antioxidant enzyme activity) and oxidative damage in *Guar*.

FHSPG1 mitigated this adverse effect of CuO. The results showed that almost all NPs significantly increased ANC, PPO, POX, CAT, and PRL levels, especially using FSMPF1, FHSPF2, FSMPG3, and FHSPG1, which significantly increased ANC, PPO, POX, CAT, and PRL levels. It is evident that ANC, PPO, POX, CAT, and PRL prevent the breakdown of macromolecules and enzyme destruction and maintain the strength of the cell wall when exposed to environmental stress. Therefore, it seems that increasing ANC, PPO, POX, CAT, and PRL, as well as ANC and PPO, intensifies this effect and increases the plant's tolerance to stress. *Phaseolus vulgaris* seedlings treated with Fe₃O₄ NPs and Si-NPs had a higher level of antioxidant content when exposed to Cd stress.⁵⁹ NP-treated seedlings may produce more antioxidants and be able to synthesize antioxidants that regulate the plant water content. Furthermore, nanoparticles

Table 6. Means Comparison of the Secondary Metabolites and Content of Elements of Guar under the Influence of Our NPs and CuO Stress^a

	treatments	N	Fe	α -pinene	α -terpinene	camphene	1,8-cineol
normal-irrigation	control	1.34 ^h	1.16 ⁱ	9.15 ^g	22.73 ^g	1.15 ⁱ	1.35 ^j
	FSM	2.76 ^g	1.73 ^h	10.16 ^f	27.24 ^f	1.74 ^g	2.76 ^{ghi}
	FHS	2.66 ^g	2.33 ^f	12.29 ^e	29.31 ^f	2.35 ^e	2.63 ^{hi}
	FSMPF	3.14 ^f	2.13 ^g	12.68 ^{de}	32.45 ^e	2.14 ^f	3.13 ^{gh}
	FHSPF	2.78 ^g	2.13 ^g	12.16 ^e	33.53 ^e	2.13 ^f	3.83 ^{def}
	FSMPG	3.16 ^{ef}	2.54 ^d	12.94 ^{cd}	37.68 ^{cd}	2.53 ^d	4.14 ^{cde}
	FHSPG	3.34 ^{ef}	2.37 ^f	13.24 ^{bc}	39.58 ^{bc}	2.36 ^e	4.35 ^{bcd}
CuO stress	control	1.61 ^h	1.32 ⁱ	7.28 ^h	27.15 ^f	1.35 ^h	2.11 ^{ij}
	FSM	3.34 ^{ef}	2.35 ^f	10.13 ^f	31.94 ^e	2.31 ^e	3.35 ^{gh}
	FHS	3.42 ^{de}	2.47 ^e	12.46 ^{de}	28.74 ^f	2.48 ^d	3.44 ^{efg}
	FSMPF	3.69 ^{cd}	2.74 ^c	12.51 ^{de}	33.56 ^e	2.74 ^c	4.75 ^{abc}
	FHSPF	3.76 ^{bc}	2.74 ^c	12.68 ^{de}	36.46 ^d	2.73 ^c	4.78 ^{abc}
	FSMPG	4.04 ^{ab}	2.9 ^b	13.78 ^b	40.92 ^b	2.96 ^b	4.97 ^{ab}
	FHSPG	4.22 ^a	3.18 ^a	14.37 ^a	47.52 ^a	3.23 ^a	5.20 ^a

^aMeans in each column followed by a similar letter(s) are not significantly different at 1% probability level, using the LSD test.

were shown to enhance proline synthesis under stress conditions in bean crops and to regulate antioxidant defenses, soluble sugar levels, and amino acid metabolism.⁶⁰

It has been demonstrated that PAs, such as spermine, increase levels of osmolytes, such as proline, under environmental stress. Under stressful conditions, PAs with single and multibranches promoted proline accumulation when applied (Tables 3 and 4). Thus, our NPs increase proline storage, free amino acid content, antioxidant enzyme activity, nutritional content, and plant tolerance to environmental stressors.^{12,14,22,51}

3.3.5. Effect of CuO Stress and Our NPs Application on Secondary Metabolites and the Content of Elements of Guar. The effects of the FSM3, FHS2, FSMPF1, FHSPF2, FSMPG3, and FHSPG1 treatments on N, Fe, α -pinene, α -terpinene, camphene, and 1,8-cineol of Guar were NPs and culture medium type dependent and are summarized in Table 5.

3.3.6. Effects of Our NPs on the Secondary Metabolites and the Content of Elements of Guar. The present study demonstrated that the application of FSM3, FHS2, FSMPF1, FHSPF2, FSMPG3, and FHSPG1 coatings had a positive effect on the contents of N, Fe, α -pinene, α -terpinene, camphene, and 1,8-cineol in Guar. The results showed that, in two types of culture medium (with and without CuO stress), the application of our NPs had a positive effect on the secondary metabolites and the content of elements in Guar compared to the control treatment. Based on the analysis of variance, the interaction effects of NPs and CS (NPs \times CS) were significant for Fe, α -pinene, α -terpinene, and camphene (Tables 5 and 6).

Multibranching PAs increased plant productivity and production compared to single-branched PAs. The results showed the high utilization efficiency of FSMPG3 and FHSPG1 compared to FSMPF1 and FHSPF2, and of FHSPG1 and FHSPF2 compared with FSMPG3 and FSMPF1, respectively. This increase in efficiency was observed in both culture media with and without CuO stress. The enhanced efficiency of FSM3 and FHS2 treatments in FSMPF1, FHSPF2, FSMPG3, and FHSPG1, as multibranching polyamines, compared with the control, highlights the strong potential of these nanoparticles to increase secondary metabolite production and elemental accumulation in guar. The observed increases in N, Fe, α -pinene, α -terpinene,

camphene, and 1,8-cineole following the FSMPG3 and FHSPG1 application in both culture media (with and without CuO-induced stress) may be attributed to elevated metabolic activity in guar. These findings are consistent with previous reports.^{12,14,22,51}

As is widely known, environmental stress affects nutrient availability, uptake, and the transfer of nutrients to plants. According to the present study, PAs treatments with single-branched or multibranching branches increased the contents of leaf nutrients and the secondary metabolites under stress conditions. In other words, the presence of CuO and the absence of NPs decrease the nutrients and secondary metabolites (Tables 2 and 5). Furthermore, NPs were found to significantly improve Fe levels under CuO stress conditions compared to their absence (Table 6). Also, FSMPG3 and FHSPG1 applied to the plants increased their Fe content. As a result of copper presence in soils, nitrogen and iron cannot move between plant parts when the plant is under heavy metal stress conditions, so secondary metabolites are not produced. This may be due to the metal transport system at the plasma membrane and the competition between metal elements for transport by this system. Under CuO stress conditions, the plant absorbed less N and Fe than in nonstress conditions. As a result of NPs, the Guar plant was able to absorb nutrients and produce secondary metabolites more efficiently. The PAs, which form amino acids in various biological reactions, appear to boost N absorption and storage in plants, shielding them from environmental stress. Apparently, spermine enhances photosynthesis and root discharge, which improves nitrogen uptake by plant roots while also producing secondary metabolites. As reported, the application of PAs such as spermine resulted in increased mineral uptake by leaf tissue.²²

By increasing the percentage of thin, hairy roots and reducing the rate of thick roots, external PAs improve the root structure. PAs are involved in the process of root growth. In addition to enhancing secondary metabolite production, these changes also increase the absorption and concentration of the elements in plants. Fe₃O₄ NPs, SM, and HS (as PAs), PEG, glucose, and folic acid, on the other hand, increase the amount of nitrogen and iron in plants by supplying them with additional sources. Moreover, studies have reported that cationic nanoparticles, such as Fe₃O₄ NPs applied with spermine or homospermine, PEG, glucose, and folic acid,

can enhance secondary metabolite concentrations and upregulate the expression of genes involved in their biosynthesis (Tables 5 and 6). Thus, secondary metabolites produced by plants are used to combat free radical damage.^{2,12,27,45,46}

4. CONCLUSIONS

This study represents the successful completion of a research project focused on the development of magnetic NPs that are both biodegradable and biocompatible with strong potential for safe application in biological systems. The synthesized NPs, namely, FSMPP1, FHSPF2, FSMPP3, and FHSPG1, were designed using eco-friendly surface functionalizations, including spermine, PEG, folic acid, and glucose. These modifications not only enhanced their gene delivery efficiency but also ensured excellent cellular compatibility and environmental safety. Experimental results demonstrated that these NPs significantly improved plant growth parameters, antioxidant enzyme activities, and nutrient uptake under abiotic stress conditions, such as exposure to copper oxide. Among them, FHSPG1 exhibited powerful protective effects by boosting antioxidant defenses and reducing hydrogen peroxide accumulation, thereby enhancing stress tolerance in Guar plants. Moreover, cytotoxicity evaluations in both plant cells and MCF-7 human cancer cells confirmed that the NPs maintained high cell viability even at concentrations up to 1000 μg per milliliter. At the optimal dose of 500 mmol/mL , they showed no adverse effects on cellular health or microbial viability. Antibacterial assessments also indicated a minimal impact on beneficial microbial populations, further confirming their environmental compatibility. Taken together, these findings introduce FSMPP1, FHSPF2, FSMPP3, and FHSPG1 as a new class of safe, nontoxic, and environmentally friendly nanocarriers. These NPs are not only effective for gene delivery and stress mitigation but also fully degradable, posing no ecological threat throughout their lifecycle. As such, they offer a promising solution for applications in sustainable agriculture, plant biotechnology, and future biomedical innovations where safety, efficiency, and environmental responsibility are essential. These effects are primarily driven by the coordinated action of the polymer coatings and functional ligands, which enhance nutrient delivery, scavenge reactive oxygen species, and activate antioxidant defense pathways, thereby improving plant resilience under abiotic stresses such as copper oxide exposure.

■ ASSOCIATED CONTENT

Data Availability Statement

The data sets generated and analyzed during the current study are available from the corresponding author upon reasonable request. Additionally, part of the data is provided in the Supporting Information file submitted to the system, and the figures are included in a separate PDF file to preserve their quality.

SI Supporting Information

The Supporting Information is available free of charge at <https://pubs.acs.org/doi/10.1021/acsomega.5c06841>.

Experimental procedures; materials; and characterization data (Tables S1–S3) (Figure S1) (PDF)

■ AUTHOR INFORMATION

Corresponding Authors

Mehdi Afrouz – Department of Plant Production and Genetics, University of Mohaghegh Ardabili, 56199-11367 Ardabil, Iran; orcid.org/0000-0003-4904-5069; Email: mehdiafrouz@uma.ac.ir

Shadi Majd-Marani – Department of Plant Production and Genetics, University of Mohaghegh Ardabili, 56199-11367 Ardabil, Iran; Email: shadimajd@uma.ac.ir

Te Ming Tseng – Department of Plant and Soil Science, Mississippi State University, Mississippi State, Mississippi 39762, United States; Email: tt1024@msstate.edu

Authors

Hoda Zahedian – Department of Deutsch-Sprachen, Volkshochschule, 33330 Gütersloh, Germany

Fateme Arabnejad – Department of Radio Oncology, Kerman University of Medical Sciences, 76169-14115 Kerman, Iran

Mohammad Taghi Alebrahim – Department of Plant Production and Genetics, University of Mohaghegh Ardabili, 56199-11367 Ardabil, Iran; orcid.org/0000-0002-6032-6470

Ali Eftekhari – Department of Supramolecular Chemistry and Nanomaterials, Tampere University, FI-33014 Tampere, Finland

Payman Azghani – School of Medicine, Ardabil University of Medical Sciences, 56189-85991 Ardabil, Iran

Complete contact information is available at:

<https://pubs.acs.org/10.1021/acsomega.5c06841>

Author Contributions

M.A.: Conceptualization, methodology, investigation, formal analysis, data curation, writing—original draft, project administration, supervision. S.M.-M.: Methodology, investigation, validation, visualization, writing—review and editing. H.Z.: Writing—review and editing, visualization, language editing. F.A.: Data curation, formal analysis, resources. M.T.A.: Supervision, funding acquisition, resources, writing—review and editing. A.E.: Resources, methodology, writing—review and editing. P.A. and T.M.T.: Conceptualization, supervision, writing—review and editing, validation.

Author Contributions

M.A. and S.M.M. conceived and designed the research, prepared the materials, collected the data, and performed the initial data analysis. S.M.M. carried out further data interpretation. M.A. wrote the first draft of the manuscript with contributions from S.M.M., H.Z., and F.A. H.Z., M.T.A., A.E., P.A., and T.M.T. provided critical revisions and comments on earlier versions of the manuscript. All authors reviewed and approved the final version of the manuscript.

Notes

The authors declare no competing financial interest.

Highlights I. Evaluation of the optimal concentration of iron oxide (Fe_3O_4) nanoparticles (NPs) and single-branched and multibranched polyamines (PAs) by spermine, PEG, glucose, and folic acid to improve germination and increase dry matter content and length of Guar (cluster) bean seedlings. II. Determining the best method of using Fe_3O_4 NPs and single-branched and multibranched PAs to improve the biochemical characteristics of the growth of Guar bean seedlings. III. Reduction of copper oxide stress on Guar through the

application of Fe₃O₄ NPs and single-branched and multi-branched PAs and their effect on plant antioxidant activity.

ACKNOWLEDGMENTS

The author wishes to thank Ivan A. Paponov (Aarhus University), Sabry G. Elias (Oregon State University), and Christophe Coudret (Université de Toulouse) for their valuable advice on various technical aspects of this work.

ABBREVIATIONS

ANC, anthocyanin; CAT, catalase; Cu NPs, copper oxide (CuO); DLS, dynamic light scattering; DMSO, dimethyl sulfoxide; EDC, 1-ethyl-3-(3-(dimethylamino)propyl)-carbodiimide; EDX, energy-dispersive X-ray fluorescence spectrometer; F, iron; FBS, fetal bovine serum; Fe NPs, iron oxide (Fe₃O₄); FHS, Fe₃O₄-hyperbranched spermine; FHSPE, Fe₃O₄-hyperbranched spermine-poly(ethylene glycol)-folic acid; FHSPG, Fe₃O₄-hyperbranched spermine-poly(ethylene glycol)-glucose; FSM, Fe₃O₄-spermine; FSMPF, Fe₃O₄-spermine-poly(ethylene glycol)-folic acid; FSMPG, Fe₃O₄-spermine-poly(ethylene glycol)-glucose; FTIR, Fourier transform infrared spectroscopy; Glu-PEG-NH₂, glucose-poly(ethylene glycol)amine; H₂O₂, hydrogen peroxide; H NMR, hydrogen nuclear magnetic resonance spectroscopy; HS, hyperbranched spermine; MBA, magnetic behavior analysis; MDA, malondialdehyde; MNPs, magnetic nanoparticles; MTT, 3-(4,5-dimethylthiazol-2-yl)-2,5-diphenyltetrazolium bromide; N, nitrogen; NL, number of leaves; NPs, nanoparticles; OP, osmotic potential; PAs, polyamines; POD, peroxidase; POX, peroxidase; PPO, polyphenol oxidase; PRL, proline; PVP, polyvinylpyrrolidone; ROS, reactive oxygen species; RV, root volume; RWC, relative water content; SEM, scanning electron microscopy; SEP, percentage of seedling establishment; SES, speed of seedling establishment; SM, spermine; SOD, superoxide dismutase; TDW, total dry weight; TEM, transmission electron microscopy; TEOS, tetraethyl orthosilicate; TGA, thermogravimetric analysis; TG-DTA, thermogravimetric measurements; TL, total length; TOA, trioctylamine; UV-vis, ultraviolet-visible spectroscopy; VSM, vibrating sample magnetometer; MSFW, Mealworm-based Spinach-Food Waste

REFERENCES

- (1) Ahmadi-Nouraldin, F.; Afrouz, M.; Elias, S. G.; Eslamian, S. Green Synthesis of Copper Nanoparticles Extracted from Guar Seedling under Cu Heavy-Metal Stress by *Trichoderma Harzianum* and Their Bio-Efficacy Evaluation against *Staphylococcus Aureus* and *Escherichia Coli*. *Environ. Earth Sci.* **2022**, *81* (2), 54.
- (2) Ahmadi-Nouraldin, F.; Afrouz, M.; Tseng, T.-M. P.; Poshtdar, A.; Coudret, C. Green Synthesis of Hyperbranched Spermine-Coated Fe₃O₄ Nanoparticles and Their Effect on Corn Seedlings under Copper Oxide Stress. *ACS Sustainable Chem. Eng.* **2023**, *11* (35), 12888–12907.
- (3) Zhang, J.; Xie, S.; Wei, Y.; Liang, Y. Physiological Responses and Uptake of Heavy Metals by *Miscanthus Sacchariflorus* (Maxim.) Benth., an Energy Plant Species, under Multiple Heavy Metals Stress. *Arch. Agron. Soil Sci.* **2021**, 259–274.
- (4) Zaheer, I. E.; Ali, S.; Rizwan, M.; Farid, M.; Shakoor, M. B.; Gill, R. A.; Najeer, U.; Iqbal, N.; Ahmad, R. Citric Acid Assisted Phytoremediation of Copper by *Brassica Napus* L. *Ecotoxicol. Environ. Saf.* **2015**, *120*, 310–317.
- (5) Ahmad, S.; Munir, S.; Zeb, N.; Ullah, A.; Khan, B.; Ali, J.; Bilal, M.; Omer, M.; Alamzeb, M.; Salman, S. M. Green Nanotechnology: A

Review on Green Synthesis of Silver Nanoparticles—An Ecofriendly Approach. *Int. J. Nanomed.* **2019**, 5087–5107.

(6) Bumbulyte, G.; Būdienė, J.; Būda, V. Essential Oils and Their Components Control Behaviour of Yellow Mealworm (*Tenebrio Molitor*) Larvae. *Insects* **2023**, *14* (7), 636.

(7) Reddiex, A. J.; Gosden, T. P.; Bonduriansky, R.; Chenoweth, S. F. Sex-Specific Fitness Consequences of Nutrient Intake and the Evolvability of Diet Preferences. *Am. Nat.* **2013**, *182* (1), 91–102.

(8) Azizi, A. Green Synthesis of Fe₃O₄ Nanoparticles and Its Application in Preparation of Fe₃O₄/Cellulose Magnetic Nanocomposite: A Suitable Proposal for Drug Delivery Systems. *J. Inorg. Organomet. Polym. Mater.* **2020**, *30* (9), 3552–3561.

(9) Biteau, C.; Bry-Chevalier, T.; Crummett, D.; Ryba, R.; Jules, M. S. Is Turning Food Waste into Insect Feed an Uphill Climb? A Review of Persistent Challenges. **2024**.

(10) Kornarzyński, K.; Sujak, A.; Czernel, G.; Wiącek, D. Effect of Fe₃O₄ Nanoparticles on Germination of Seeds and Concentration of Elements in *Helianthus Annuus* L. under Constant Magnetic Field. *Sci. Rep.* **2020**, *10* (1), 8068.

(11) Bergonci, T.; Fomsgaard, I. S.; Kjaer, K. H.; Paponov, I. A. Hormone-Flavonoid Patterns in Two Genotypes of *Campanula Portenschlagiana* with Distinct Adventitious Rooting Competence. *Horticulturae* **2023**, *9* (1), 121.

(12) Afrouz, M.; Ahmadi-Nouraldin, F.; Elias, S. G.; Alebrahim, M. T.; Tseng, T. M.; Zahedian, H. Green Synthesis of Spermine Coated Iron Nanoparticles and Its Effect on Biochemical Properties of *Rosmarinus Officinalis*. *Sci. Rep.* **2023**, *13* (1), 775.

(13) Tyagi, A.; Ali, S.; Ramakrishna, G.; Singh, A.; Park, S.; Mahmoudi, H.; Bae, H. Revisiting the Role of Polyamines in Plant Growth and Abiotic Stress Resilience: Mechanisms, Crosstalk, and Future Perspectives. *J. Plant Growth Regul.* **2023**, *42* (8), 5074–5098.

(14) Hasan, M. M.; Skalicky, M.; Jahan, M. S.; Hossain, M.; Anwar, Z.; Nie, Z.-F.; Alabdallah, N. M.; Brestic, M.; Hejnak, V.; Fang, X.-W. Spermine: Its Emerging Role in Regulating Drought Stress Responses in Plants. *Cells* **2021**, *10* (2), 261.

(15) Jiang, H.-L.; Xing, L.; Luo, C.-Q.; Zhou, T.-J.; Li, H.-S.; Cho, C.-S. Chemical Modification of Chitosan as a Gene Transporter. *Curr. Org. Chem.* **2018**, *22* (7), 668–689.

(16) Yuan, W.; Li, H. Polymer-Based Nanocarriers for Therapeutic Nucleic Acids Delivery. In *Nanostructures for Drug Delivery*; Elsevier, 2017; pp 445–460.

(17) Zhang, M.; Kim, Y. K.; Cui, P.; Zhang, J.; Qiao, J.; He, Y.; Lyu, J.; Luo, C.; Xing, L.; Jiang, H. Folate-Conjugated Polyspermine for Lung Cancer-Targeted Gene Therapy. *Acta Pharm. Sin B* **2016**, *6* (4), 336–343.

(18) Luo, Y.; Zhu, S.; Peng, J.; Cui, H.; Huang, Q.; Xu, B.; Ho, C.-T. Feasibility Study of Amadori Rearrangement Products of Glycine, Diglycine, Triglycine, and Glucose as Potential Food Additives for Production, Stability, and Flavor Formation. *J. Agric. Food Chem.* **2024**, *72* (1), 657–669.

(19) Yan, Z.; Tang, Y.; Zhang, Z.; Feng, J.; Hao, J.; Sun, S.; Li, M.; Song, Y.; Dong, W.; Hu, L. Biocompatible Folic-Acid-Strengthened Ag–Ir Quantum Dot Nanozyme for Cell and Plant Root Imaging of Cysteine/Stress and Multichannel Monitoring of Hg²⁺ and Dopamine. *Anal. Chem.* **2024**, *96* (10), 4299–4307.

(20) Biresaw, S. S.; Taneja, P. Copper Nanoparticles Green Synthesis and Characterization as Anticancer Potential in Breast Cancer Cells (MCF7) Derived from *Prunus Nepalensis* Phytochemicals. *Mater. Today Proc.* **2022**, *49*, 3501–3509.

(21) Ahmadi-Nouraldin, F.; Afrouz, M.; Tseng, T.-M. P.; Poshtdar, A.; Coudret, C. Green Synthesis of Hyperbranched Spermine-Coated Fe₃O₄ Nanoparticles and Their Effect on Corn Seedlings under Copper Oxide Stress. *ACS Sustainable Chem. Eng.* **2023**, *11* (35), 12888–12907.

(22) Lechowska, K.; Wojtyła, E.; Quinet, M.; Kubala, S.; Lutts, S.; Garnczarska, M. Endogenous Polyamines and Ethylene Biosynthesis in Relation to Germination of Osmoprimed *Brassica Napus* Seeds under Salt Stress. *Int. J. Mol. Sci.* **2022**, *23* (1), 349.

- (23) Afrouz, M.; Amani, A.; Eftekhari, A.; Coudret, C.; Elias, S. G.; Ahmadian, Z.; Alebrahim, M. T. Design and Synthesis of Multi-Targeted Nanoparticles for Gene Delivery to Breast Cancer Tissues. *Naunyn-Schmiedeberg's Arch. Pharmacol.* **2023**, *396* (1), 121–137.
- (24) Afrouz, M.; Ahmadi-Nouraldin, F.; Elias, S. G.; Alebrahim, M. T.; Tseng, T. M.; Zahedian, H. Green Synthesis of Spermine Coated Iron Nanoparticles and Its Effect on Biochemical Properties of *Rosmarinus Officinalis*. *Sci. Rep.* **2023**, *13* (1), 775.
- (25) Sonawane, N. D.; Szoka, F. C.; Verkman, A. S. Chloride Accumulation and Swelling in Endosomes Enhances DNA Transfer by Polyamine-DNA Polyplexes. *J. Biol. Chem.* **2003**, *278* (45), 44826–44831.
- (26) Samanta, I.; Roy, P. C.; Das, E.; Mishra, S.; Chowdhary, G. Plant Peroxisomal Polyamine Oxidase: A Ubiquitous Enzyme Involved in Abiotic Stress Tolerance. *Plants* **2023**, *12* (3), 652.
- (27) Blázquez, M. A. Polyamines: Their Role in Plant Development and Stress. *Annu. Rev. Plant Biol.* **2024**, *75* DOI: [10.1146/annurev-arplant-070623-110056](https://doi.org/10.1146/annurev-arplant-070623-110056).
- (28) Majd-Marani, S.; Eftekhari, A.; Elias, S. G.; Beffa, R.; Alebrahim, M. T.; Mishra, A. P.; Afrouz, M. A Novel Approach in Using Insect-Based Spinach-Food Waste for Gene Targeting to Cancer Tissues. *Sci. Rep.* **2025**, *15* (1), No. 13905.
- (29) Abebe, D. G.; Kandil, R.; Kraus, T.; Elsayed, M.; Merkel, O. M.; Fujiwara, T. Three-Layered Biodegradable Micelles Prepared by Two-Step Self-Assembly of PLA-PEI-PLA and PLA-PEG-PLA Triblock Copolymers as Efficient Gene Delivery System. *Macromol. Biosci.* **2015**, *15* (5), 698–711.
- (30) Duan, Q.; Liu, R.; Luo, J.-Q.; Zhang, J.-Y.; Zhou, Y.; Zhao, J.; Du, J.-Z. Virus-Inspired Glucose and Polydopamine (GPDA)-Coating as an Effective Strategy for the Construction of Brain Delivery Platforms. *Nano Lett.* **2024**, *24* (1), 402–410.
- (31) Amani, A.; Alizadeh, M. R.; Yaghoubi, H.; Nohtani, M. Novel Multi-Targeted Nanoparticles for Targeted Co-Delivery of Nucleic Acid and Chemotherapeutic Agents to Breast Cancer Tissues. *Mater. Sci. Eng. C* **2021**, *118* (2020), No. 111494.
- (32) Afrouz, M.; Ahmadi-Nouraldin, F.; Amani, A.; Zahedian, H.; Elias, S. G.; Arabnejad, F.; Yaghoubi, H.; Farshad, O.; Farazi, N.; Jalali, A. Preparation and Characterization of Magnetic PEG-PEI-PLA-PEG/FeO₄-PCL/DNA Micelles for Gene Delivery into MCF-7 Cells. *J. Drug Delivery Sci. Technol.* **2022**, No. 104016.
- (33) Afrouz, M.; Amani, A.; Eftekhari, A.; Coudret, C.; Elias, S. G.; Ahmadian, Z.; Alebrahim, M. T. Design and Synthesis of Multi-Targeted Nanoparticles for Gene Delivery to Breast Cancer Tissues. *Naunyn-Schmiedeberg's Arch. Pharmacol.* **2023**, *396* (1), 121–137.
- (34) Afrouz, M.; Ahmadi-Nouraldin, F.; Ajirlu, Y. Y.; Arabnejad, F.; Eskanlou, H.; Yaghoubi, H. Preparation and Characterization of PLA-PEG/Chitosan-FA/DNA for Gene Transfer to MCF-7 Cells. *Med. Drug Discovery* **2022**, *15*, No. 100138.
- (35) Afrouz, M.; Amani, A.; Eftekhari, A.; Coudret, C.; Elias, S. G.; Ahmadian, Z.; Alebrahim, M. T. Design and Synthesis of Multi-Targeted Nanoparticles for Gene Delivery to Breast Cancer Tissues. *Naunyn-Schmiedeberg's Arch. Pharmacol.* **2023**, *396* (1), 121–137.
- (36) Afrouz, M.; Ahmadi-nouraldin, F.; Amani, A.; Zahedian, H.; Jalali, A.; Eskanlou, H. Journal of Drug Delivery Science and Technology Preparation and Characterization of Magnetic PEG-PEI-PLA-PEG/Fe₃O₄-PCL/DNA Micelles for Gene Delivery into MCF-7 Cells. *J. Drug Delivery Sci. Technol.* **2023**, *79* (2022), No. 104016.
- (37) Afrouz, M.; Ahmadi-Nouraldin, F.; Amani, A.; Zahedian, H.; Elias, S. G.; Arabnejad, F.; Yaghoubi, H.; Farshad, O.; Farazi, N.; Jalali, A. Preparation and Characterization of Magnetic PEG-PEI-PLA-PEG/FeO₄-PCL/DNA Micelles for Gene Delivery into MCF-7 Cells. *J. Drug Delivery Sci. Technol.* **2022**, No. 104016.
- (38) Lv, Y.; Xue, J.; Cui, P.; Qiu, L. Spermine Significantly Increases the Transfection Efficiency of Cationic Polymeric Gene Vectors. *Pharmaceutics* **2025**, *17* (1), 131.
- (39) Angelopoulou, A.; Kolokithas-Ntoukas, A.; Fytas, C.; Avgoustakis, K. Folic Acid-Functionalized, Condensed Magnetic Nanoparticles for Targeted Delivery of Doxorubicin to Tumor Cancer Cells Overexpressing the Folate Receptor. *ACS Omega* **2019**, *4* (26), 22214–22227.
- (40) Campos, M. T.; Pires, L. S.; Magalhaes, F. D.; Oliveira, M. J.; Pinto, A. Self-Assembled Inorganic Nanomaterials for Biomedical Applications. *Nanoscale* **2025**, *17*, 5526–5570, DOI: [10.1039/D4NR04537H](https://doi.org/10.1039/D4NR04537H).
- (41) Safari Sharafshadeh, M.; Tafvizi, F.; Khodarahmi, P.; Ehteshami, S. Folic Acid-Functionalized PEGylated Niosomes Co-Encapsulated Cisplatin and Doxorubicin Exhibit Enhanced Anticancer Efficacy. *Cancer Nanotechnol.* **2024**, *15* (1), 14.
- (42) Puangpathumanond, S.; Chee, H. L.; Sevensan, C.; Yang, X.; Lau, O. S.; Lew, T. T. S. Stomata-Targeted Nanocarriers Enhance Plant Defense against Pathogen Colonization. *Nat. Commun.* **2025**, *16* (1), 4816.
- (43) Tasnim, N. T.; Ferdous, N.; Rumon, M. M. H.; Shakil, M. S. The Promise of Metal-Doped Iron Oxide Nanoparticles as Antimicrobial Agent. *ACS Omega* **2024**, *9* (1), 16–32.
- (44) Stassinis, P. M.; Rossi, M.; Borromeo, I.; Capo, C.; Beninati, S.; Forni, C. Enhancement of Brassica Napus Tolerance to High Saline Conditions by Seed Priming. *Plants* **2021**, *10* (2), 403.
- (45) Kolesnikov, Y. S.; Kretynin, S. V.; Filepova, R.; Dobrev, P. I.; Martinec, J.; Kravets, V. S. Polyamines Metabolism and Their Biological Role in Plant Cells: What Do We Really Know? *Phytochem. Rev.* **2024**, *23*, 997–1026.
- (46) Schibalski, R. S.; Shulha, A. S.; Tsao, B. P.; Palygin, O.; Ilatovskaya, D. V. The Role of Polyamine Metabolism in Cellular Function and Physiology. *Am. J. Physiol.-Cell Physiol.* **2024**, *327* (2), C341–C356.
- (47) Zhao, G.-c.; Xie, M.; Wang, Y.; Li, J. Molecular Mechanisms Underlying γ -Aminobutyric Acid (GABA) Accumulation in Giant Embryo Rice Seeds. *J. Agric. Food Chem.* **2017**, *65* (24), 4883–4889.
- (48) Nahar, K.; Rahman, M.; Hasanuzzaman, M.; Alam, M. M.; Rahman, A.; Suzuki, T.; Fujita, M. Physiological and Biochemical Mechanisms of Spermine-Induced Cadmium Stress Tolerance in Mung Bean (*Vigna radiata* L.) Seedlings. *Environ. Sci. Pollut. Res.* **2016**, *23*, 21206–21218.
- (49) Creff, A.; Ali, O.; Bied, C.; Bayle, V.; Ingram, G.; Landrein, B. Evidence That Endosperm Turgor Pressure Both Promotes and Restricts Seed Growth and Size. *Nat. Commun.* **2023**, *14* (1), No. 67.
- (50) Tian, J.; Zhao, Y.; Pan, Y.; Chen, X.; Wang, Y.; Lin, J.; Wang, J.; Yang, Q. Exogenous Applications of Spermidine Improve Drought Tolerance in Seedlings of the Ornamental Grass *Hordeum jubatum* in Northeast China. *Agronomy* **2022**, *12* (5), 1180.
- (51) Chen, D.; Shao, Q.; Yin, L.; Younis, A.; Zheng, B. Polyamine Function in Plants: Metabolism, Regulation on Development, and Roles in Abiotic Stress Responses. *Front. Plant Sci.* **2019**, *9*, 1945.
- (52) Yuan, H.; Liu, Q.; Fu, J.; Wang, Y.; Zhang, Y.; Sun, Y.; Tong, H.; Dhankher, O. P. Co-Exposure of Sulfur Nanoparticles and Cu Alleviate Cu Stress and Toxicity to Oilseed Rape *Brassica napus* L. *J. Environ. Sci.* **2023**, *124*, 319–329.
- (53) Das, K. C.; Misra, H. P. Hydroxyl Radical Scavenging and Singlet Oxygen Quenching Properties of Polyamines. *Mol. Cell. Biochem.* **2004**, *262*, 127–133.
- (54) Manara, A. Plant Responses to Heavy Metal Toxicity. *Plants Heavy Metals* **2012**, 27–53.
- (55) Paciolla, C.; Paradiso, A.; de Pinto, M. C. Cellular Redox Homeostasis as Central Modulator in Plant Stress Response. In *Redox State as a Central Regulator of Plant-Cell Stress Responses*; Springer International Publishing: Cham, 2016; pp 1–23.
- (56) Groppa, M. D.; Tomaro, M. L.; Benavides, M. P. Polyamines as Protectors against Cadmium or Copper-Induced Oxidative Damage in Sunflower Leaf Discs. *Plant Sci.* **2001**, *161* (3), 481–488.
- (57) Murray Stewart, T.; Dunston, T. T.; Woster, P. M.; Casero, R. A., Jr Polyamine Catabolism and Oxidative Damage. *J. Biol. Chem.* **2018**, *293* (48), 18736–18745.
- (58) Andrés, C. M. C.; Pérez de la Lastra, J. M.; Juan, C. A.; Plou, F. J.; Pérez-Lebeña, E. Chemistry of Hydrogen Peroxide Formation and Elimination in Mammalian Cells, and Its Role in Various Pathologies. *Stresses* **2022**, *2* (3), 256–274.

(59) Koleva, L.; Umar, A.; Yasin, N. A.; Shah, A. A.; Siddiqui, M. H.; Alamri, S.; Riaz, L.; Raza, A.; Javed, T.; Shabbir, Z. Iron Oxide and Silicon Nanoparticles Modulate Mineral Nutrient Homeostasis and Metabolism in Cadmium-Stressed *Phaseolus Vulgaris*. *Front. Plant Sci.* **2022**, *13*, No. 806781.

(60) Nasrallah, A. K.; Kheder, A. A.; Kord, M. A.; Fouad, A. S.; El-Mogy, M. M.; Atia, M. A. M. Mitigation of Salinity Stress Effects on Broad Bean Productivity Using Calcium Phosphate Nanoparticles Application. *Horticulturae* **2022**, *8* (1), 75.



CAS BIOFINDER DISCOVERY PLATFORM™

**ELIMINATE DATA
SILOS. FIND
WHAT YOU
NEED, WHEN
YOU NEED IT.**

A single platform for relevant,
high-quality biological and
toxicology research

Streamline your R&D

CAS
A division of the
American Chemical Society